

# **Advanced Composites as Reinforcement for Concrete**

مركبات متطورة كتقوية للخرسانة المسلحة

by

**IBRAHIM AL SAMARAIE**

**Dissertation submitted in fulfilment  
of the requirements for the degree of  
MSc STRUCTURAL ENGINEERING**

at

**The British University in Dubai**

**May 2021**

## DECLARATION

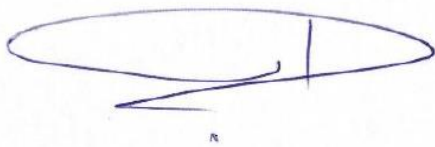
I warrant that the content of this research is the direct result of my own work and that any use made in it of published or unpublished copyright material falls within the limits permitted by international copyright conventions.

I understand that a copy of my research will be deposited in the University Library for permanent retention.

I hereby agree that the material mentioned above for which I am author and copyright holder may be copied and distributed by The British University in Dubai for the purposes of research, private study or education and that The British University in Dubai may recover from purchasers the costs incurred in such copying and distribution, where appropriate.

I understand that The British University in Dubai may make a digital copy available in the institutional repository.

I understand that I may apply to the University to retain the right to withhold or to restrict access to my thesis for a period which shall not normally exceed four calendar years from the congregation at which the degree is conferred, the length of the period to be specified in the application, together with the precise reasons for making that application.

A handwritten signature in blue ink, consisting of a large, stylized loop followed by a vertical line and a horizontal stroke.

---

Signature of the student

## **COPYRIGHT AND INFORMATION TO USERS**

The author whose copyright is declared on the title page of the work has granted to the British University in Dubai the right to lend his/her research work to users of its library and to make partial or single copies for educational and research use.

The author has also granted permission to the University to keep or make a digital copy for similar use and for the purpose of preservation of the work digitally.

Multiple copying of this work for scholarly purposes may be granted by either the author, the Registrar or the Dean only.

Copying for financial gain shall only be allowed with the author's express permission.

Any use of this work in whole or in part shall respect the moral rights of the author to be acknowledged and to reflect in good faith and without detriment the meaning of the content, and the original authorship.

## **Abstract**

Recently, the demand for building concrete structures reinforced with steel rebars is gradually increasing worldwide. The serviceability of these reinforced concrete structures is affected by multiple factors, one of which is exposure to extreme weather conditions. Deterioration of steel rebars is one of the most common issues caused by the harsh environment's weather. The degradation of concrete structure is mainly driven by steel corrosion.

Fiber-reinforced polymer (FRP) rebar is considered an innovative and durable choice rather than conventional steel reinforcement for concrete structures. GFRP bars were classified as an excellent corrosion resistance compared to conventional steel due to their mechanical performance. Several researchers have performed numerous studies out to explore the flexural response of GFRP bars.

As a result, it is crucial to establish effective FE models that can be employed to comprehend the essential structural behavior of such systems and the performance under applied loads. The flexural behavior of structural reinforced concrete beam components was presented in this study utilizing 3D ANSYS 21 FEA simulation. This study compares an FE model with experimental findings from previous works and the ACI 440.1 model. Graphical representations were discussed, including the deflection of the mid-span stress-strain relationship.

The specimens are rectangular beams that are simply supported and have spans and clear spans of 2.4 m and 2.1 m. A four-point pseudo-static experiment was performed on the samples. The findings indicate that fibre-reinforced composites can be evaluated using

“

ANSYS software with an adjusted model. The difference between FEA model results, experimental tests, and ACI 440.1 theoretical formulas predicting failure loads is within a 10% margin of error. The results have demonstrated the ACI 440.1 code conservatism compared to the remainder of the results obtained from environmental findings or FE simulations.

## المخلص

في الآونة الأخيرة ، يزداد الطلب على بناء الهياكل الخرسانية المقواة بقضبان حديدية تدريجياً في جميع أنحاء العالم. تتأثر قابلية الخدمة لهذه الهياكل الخرسانية المسلحة بعدة عوامل ، أحدها التعرض لظروف الطقس القاسية. يعد تدهور حديد التسليح أحد أكثر المشكلات شيوعاً التي تسببها البيئة القاسية. إن تدهور الهيكل الخرساني ناتج بشكل أساسي عن تآكل الفولاذ.

تعتبر قضبان البوليمرات المقوى بالألياف (FRP) خياراً مبتكراً ودائماً، بدلاً من حديد التسليح الفولاذي التقليدي للهياكل الخرسانية. تم تصنيف قضبان GFRP على أنها ذات مقاومة ممتازة للتآكل مقارنة بالفولاذ التقليدي بسبب أدائها الميكانيكي.

أجرى العديد من الباحثين العديد من الدراسات لاستكشاف سلوك الانحناء لقضبان بوليمرات الزجاج المقواة بالألياف GFRP.

نتيجة لذلك ، من الضروري إنشاء نماذج فعالة للعناصر المحدودة لاستخدامها لفهم اسس الاستجابة الهيكلية للهياكل المعززة بقضبان البوليمرات المقواة بالزجاج GFRP وكيفية أدائها في ظل الأحمال المطبقة عليها. تم عرض سلوك الانحناء لمكونات الكامرة للهياكل الخرسانية في هذه الدراسة باستخدام برنامج المحاكاة انسيس اصدار 2021 لتحليل العناصر المحدودة. تقارن هذه الدراسة بين نموذج العناصر المحدودة والنتائج التجريبية المختبرية من الاعمال السابقة ونموذج المعهد الامريكي للخرسانة ACI 440.1. تمت مناقشة التمثيلات الرسومية ، بما في ذلك منحنى الانحراف متوسط المدى ومنحنى الإجهاد والانفعال.

العينات عبارة عن عوارض مستطيلة ومدعومة ببساطة بامتداد وامتداد واضح يبلغ 2.4 متر و 2.1 متر ، على التوالي. تم إخضاع العينات لتجربة شبه ثابتة من أربع نقاط. تشير النتائج إلى أنه يمكن تقييم المركبات المقواة بالألياف باستخدام برنامج المحاكاة انسيس بنموذج معدل. يقع الفرق بين نتائج نموذج العناصر التحليلية المحدودة والاختبارات التجريبية المختبرية والصيغ النظرية لنموذج المعهد الامريكي للخرسانة ACI 440.1 التي تنتبأ بأحمال الفشل ضمن هامش خطأ بنسبة 10%. أظهرت النتائج مدى تحفظ نموذج المعهد الامريكي للخرسانة ACI 440.1 مقارنة ببقية النتائج التي تم الحصول عليها من

النتائج التجريبية المختبرية أو نتائج محاكاة العناصر المحدودة FE.

## Acknowledgements

In the name of Allah, the Most Gracious, the Most Merciful.

Praise be to Allah, who by His grace good deeds are done. I write these lines, and I am very happy and glad that Allah has helped me complete this work, and I pray that he blesses this work and makes it a beacon of light that benefits the country and all people. I would like to thank my professors, Dr. Gul Ahmed Jokhio, in his capacity as the thesis supervisor and Professor Abid Abu-Tair in his capacity as a co-supervisor of the thesis.

I also will not forget everyone that helped me, after Allah, my friends in my academic career who were the best of support, on top of them my brother and friend with golden touches, Eng. Abdalla Elbana and the brother and creative friend Eng. Omar Ahmed Bakr. I also thank my muse and my sweetheart, my grandmother Nahida, who, no matter what letters I wrote, I will not do her justice. I also thank my father and my mother, may Allah protect them and help me be a good son for them. I also thank my wife and my companion in my path, Noor, for bearing me throughout the thesis process. I also thank my grandfather, uncle, and dear aunt and all of my family members. I would like to thank my relatives for always being there for my companions in this journey, my friends, Eng and me. Hassan Mualla, Eng. Mohammed Siraj, Eng. Mustafa Al-Taie, Eng. Mohammed Al Halabi, Eng. Muataz Al-Daini, Eng. Hazem Al-Farra, Eng. Abdul Rahman Al-Khalidi, Eng. Marwan Al-Othman, Eng. Hassan Shamsi, Eng. Ali Al-Naqbi, Eng. Hussein Fahmy, Eng. Omar Al-Turk, Eng. Sultan Al-Shamsi, Eng. Ahmed Al-Taniji, Eng. Imran Al-Otaibi, Eng. Samy Omar, Eng. Abdul Majid Kawaf, Eng. Nadia Nassif, Eng. Noran, my colleagues at work, and every person who supported me throughout my academic career, and may Allah grant everyone success.

Done with the grace of Alla on:

2021 AD

1442 of the Hijri year

My gratitude and appreciation

Ibrahim al-Samarrai

# Contents

- 1. Introduction ..... 1
  - 1.1. Objectives ..... 4
  - 1.2. Research significance and novelty ..... 5
- 2. Chapter 2: Literature Review ..... 7
  - 2.1. Durability ..... 7
  - 2.2. Bond Strength..... 10
  - 2.3. Shear and Flexural Strength ..... 16
  - 2.4. Design philosophy ..... 20
    - 2.4.1. Flexural Design ..... 20
    - 2.4.2. Shear Design ..... 26
  - 2.5. Design Applications ..... 30
  - 2.6. ACI Formulation..... 31
  - 2.7. Finite Element..... 33
- 3. Chapter 3: Finite Elements Modeling..... 36
  - 3.1 Case study..... 36
  - 3.2. Test Set up ..... 38
  - 3.3. Materials specifications..... 39
  - 3.4. Types of Elements ..... 41
  - 3.5. Meshing: ..... 43
- 4. Chapter 4: Results..... 46
  - 4.1. Non-Linear results ..... 46
  - 4.2. Load Deflection..... 47
  - 4.3. Loads at First Cracking..... 53
  - 4.4. At failure loads..... 54
  - 4.5. Tensile Strain of FRP ..... 54
  - 4.6. Experimental findings..... 58
    - 4.6.1. Types of failure ..... 58
    - 4.6.2. Cracking patterns..... 59
    - 4.6.3. Strain development ..... 60
- 5. Chapter 5: Discussion of Results..... 64

..

6. Chapter 6: Summary and Conclusion .....	73
7. References .....	75
8. Appendix .....	82
8.1. Appendix A .....	82
8.2. Appendix B.....	85
8.3. Appendix C.....	87

^^

## List of Tables

<b>Table 1: Beam properties that have been tested</b>	<b>36</b>
<b>Table 2 Concrete properties for ANSYS Finite Element Modeling</b>	<b>39</b>
<b>Table 3 GFRP mechanical properties and characteristics</b>	<b>40</b>
<b>Table 4: The expression of the Elements</b>	<b>43</b>
<b>Table 5: Accuracy and Comparison of Theoretical model (ACI), Experimental Work and ANSYS at initial cracking load</b>	<b>53</b>
<b>Table 6: Accuracy and Comparison of Theoretical model (ACI), Experimental Work and ANSYS at failure load</b>	<b>54</b>
<b>Table 7: The “R” coefficient of the three models</b>	<b>66</b>
<b>Table 8: Outcomes of the ANOVA single factor assessment</b>	<b>69</b>

## List of Figures

<b>Figure 1: Distribution of strain and stress under ultimate instances.[77]</b>	<b>22</b>
<b>Figure 2: The strength reducing factor as a function of reinforcement proportion [77].</b>	<b>24</b>
<b>Figure 3:Reinforcement details of the tested beam</b>	<b>37</b>
<b>Figure 4:Test details</b>	<b>38</b>
<b>Figure 5: Actual test set up</b>	<b>39</b>
<b>Figure 6 GFRP rebar stress-strain relationship</b>	<b>40</b>
<b>Figure 7: Geometry of the SOLID185element</b>	<b>41</b>
<b>Figure 8: Geometry of the REINF264 element</b>	<b>42</b>
<b>Figure 9: Coordinate System of the REINF264 element</b>	<b>42</b>
<b>Figure 10: strain-gages spots</b>	<b>44</b>
<b>Figure 11 Iterative Newton-Raphson result (2 load increments) (ANSYS)</b>	<b>46</b>
<b>Figure 12: Slopes of load-deflection for the FE and experimental findings</b>	<b>48</b>
<b>Figure 13: Slopes of load-deflection for the FE and ACI 440.1 models</b>	<b>49</b>
<b>Figure 14: Load-Deflection Plots of FE model, experimental samples, and ACI code</b>	<b>50</b>
<b>Figure 15: the beam under applied load</b>	<b>52</b>
<b>Figure 16: the beam after applied load</b>	<b>52</b>
<b>Figure 17: Tensile stress-strain curve of GFRP rebar for experimental and FE model</b>	<b>54</b>
<b>Figure 18: The stress of GFRP rebar (ANSYS 2021)</b>	<b>55</b>
<b>Figure 19: The strain of GFRP rebar (ANSYS 2021)</b>	<b>56</b>
<b>Figure 20: Compressive stress-strain curve of concrete of FE model</b>	<b>56</b>
<b>Figure 21: The stress of Concrete (ANSYS 2021)</b>	<b>57</b>
<b>Figure 22:The strain of Concrete (ANSYS 2021)</b>	<b>57</b>
<b>Figure 23: Beam at failure mode</b>	<b>58</b>
<b>Figure 24: Cracking patterns of OPCC beam</b>	<b>59</b>
<b>Figure 25:Cracking patterns of Actual OPCC beam</b>	<b>59</b>
<b>Figure 26: The flexural of GFRP rebar Load-Strain curve</b>	<b>60</b>
<b>Figure 27: the load-strain curve of un-cracked condition beam</b>	<b>61</b>
<b>Figure 28. Profile of strain across the midsection's depth.</b>	<b>62</b>
<b>Figure 29: Linear trend line of experimental correlation</b>	<b>64</b>
<b>Figure 30: Linear trend line of FE Model correlation</b>	<b>65</b>
<b>Figure 31: Linear trend line of ACI 440.1 Code Model correlation</b>	<b>65</b>
<b>Figure 32: Linear trend line of Strain-Stress correlation of Concrete by FE Model</b>	<b>67</b>
<b>Figure 33:: Linear trend line of Stress-Strain correlation of GFRP rebar gained from FE Model</b>	<b>68</b>
<b>Figure 34: Critical Value of F-distribution 2.68</b>	<b>70</b>

<b>Nomenclature</b>	
$(\Delta i)_{sus}$	Instantaneous deflection due to sustained loads
$A_{fv}$	within spacing $s$ , shear reinforcement in FRP
$f_f$	FRP reinforcement tensile stress, psi (MPa)
$f_{fb}$	the bent part of FRP reinforcement strength
$f_{fu}$	FRP tensile strength
$f_{fv}$	Smallest tensile strength design  $f_{fu}$ , the strength of the bent segment of FRP stirrups $f_{fb}$ , or relating stress to $0.004E_f$ , psi, the tensile strength of FRP for shear design (MPa)
$\epsilon_{cu}$	ultimate concrete strain
$\phi$	strength reduction factor
$a$	similar rectangular stress blocks depth, in (mm)
$A_f$	FRP reinforcement area
$b$	The rectangular cross-section width in (mm)
$b_w$	Web width
$C$	cover dimension or spacing
$C_b$	in. (mm) length between maximum compression fibre to neutral axis under balanced strain
$d$	The effective depth of the member
$E_c$	Concrete modulus of elasticity (MPa)
$E_f$	Guaranteed FRP elastic modulus
$f_c'$	Concrete compressive strength
$f_r$	GFRP rebars Stress (MPa)

..

<b>h</b>	The height of the flexural beam, in. (mm)
<b>I<sub>cr</sub></b>	moment of inertia of the transformed cracked sections
<b>I<sub>e</sub></b>	Effective moment of inertia
<b>I<sub>g</sub></b>	Gross moment of inertia
<b>K</b>	the relation between the neutral axis depth to reinforcement
<b>M<sub>a</sub></b>	The maximal moment in the member
<b>M<sub>cr</sub></b>	Moment of crack (N-mm)
<b>M<sub>n</sub></b>	the nominal capacity of the moment (N-mm)
<b>M<sub>u</sub></b>	sectional factored moment, (N-mm)
<b>n<sub>f</sub></b>	The modulus of elasticity proportion of FRP rebar to concrete
<b>S</b>	longitudinal FRP bar spacing and continuous spirals stirrup spacing or pitch
<b>V<sub>c</sub></b>	Nominal shear strength of concrete.
<b>V<sub>f</sub></b>	shear resistance of FRP stirrups.
<b>V<sub>u</sub></b>	section shear force factored
<b>β<sub>d</sub></b>	reduction coefficient used in the calculation of deflection
<b>ρ<sub>f</sub></b>	FRP reinforcement ratio
<b>ρ<sub>fb</sub></b>	The reinforcing ratio of FRP results in balanced strain conditions.
<b>β<sub>1</sub></b>	0.85 it is the concrete strength factor $f_c'$ as much as and including 4000 psi (28 MPa). The factor is continually lowered at a rate of 0.05 every 1000 psi (7 MPa) of strength more than 4000 psi (28 MPa) for strength more than 4000 psi (28 MPa), but not less than 0.65.

<b>Terminology</b>	
<b>ACI 440.1</b>	Design and Construction Manual for Fiber-Reinforced Polymer Bar-Reinforced Structural Concrete
<b>ANSYS</b>	ANSYS engineering simulator and 3d model program offers comprehensive modelling solutions with unmatched scalability and a robust multiphase
<b>Brittle</b>	The term "Brittle materials" refers to solid materials influenced by stress but show minimal plastic deformation.
<b>Composite material</b>	Composite material is a composite of two substances of distinct physical and chemical properties.
<b>Compressive Strength</b>	It is the potential of a structure to withstand loads applied to the surface without fracturing or deflection.
<b>Concrete</b>	it is a combined substantial made of cement, fine and coarse aggregates, mixed with water.
<b>Concrete Crushing</b>	It is a type of failure mode that occurs when the beam (over-reinforced section)
<b>Corrosion</b>	Corrosion is the degradation of a substrate caused by a chemical reaction with its surroundings.
<b>Ductility</b>	It is a measure of the ability of materials to deform plastically before fracture
<b>Durability</b>	Durability is described as a material's potential to stay useable in its external environment during its life cycle without disruption or an unexpected repair.
<b>Epoxy</b>	Epoxy is one of the most acceptable adhesives used for industrial applications.

<b>FEA</b>	Finite element analysis is a numerical tool for predicting how a component or structure would perform under such circumstances.
<b>Fibre</b>	The fibres provide the stiffness and strength of FRP composites.  In the fibre path, the composites are much more rigid and stiffer.
<b>Flexural strength</b>	The flexural strength is known as the maximum bending stress that a material can withstand before yielding.
<b>Four-point bending static test</b>	It is a test that is used to evaluate a specimen's flexural strength.
<b>FRP</b>	Fibre Reinforced Polymer is a polymer matrix reinforced with fibres composite material either from glass, carbon, basalt, and aramid
<b>GFRP</b>	GFRP is formed of glass fibres and has moduli of elasticity under tension 20 to 25% of steel reinforcement.
<b>GFRP Rupture</b>	It is a type of failure mode that occurs when the beam (under-reinforced section)
<b>linear-elasticity</b>	The linear-elasticity describes how rigid structures bend and become internally stressed as a result of specified loading conditions
<b>Matrix</b>	The matrix directs the loads to the fibres while also providing toughness, impact, and abrasion resistance.
<b>Modulus of elasticity</b>	It is a proportion of applying stresses to strain, and it also indicates the tendency of concrete to deflect elastically.

<b>over-reinforced section</b>	In an over-reinforced section, the percentage of reinforcement delivered exceeds the balanced section.
<b>Passion ratio</b>	A substance tends to extend in the direction perpendicular to its compression path
<b>RC</b>	Reinforced concrete beams are structural components that carry external transverse loads.
<b>Renif 264</b>	Type of element in ANSYS software usually used to simulate the bars, and it has distinct characteristics
<b>Resin</b>	It is an adhesive component that is bound to the matrix and fibre. Resin has an evident bond to the service life of the reinforced members.
<b>Serviceability</b>	According to the serviceability term, a concrete construction must be serviceable and perform its intended purpose for the duration of its working life.
<b>Shear strength</b>	Shear strength is the ability of a material that determines its resistance to a shear load before it fails in shear.
<b>SOLID185</b>	Type of element in ANSYS software usually used to simulate the concrete, and it has outstanding properties
<b>stiffness</b>	That is the degree of the body's resistance to deformation as force is applied to it.
<b>Strain</b>	Strain is the substance deflection or displacement caused by imposed stress
<b>Strength</b>	It is a measure of the stress material can withstand
<b>Stress</b>	Stress is definite as an applied force per unit area.
<b>Toughness</b>	It is a measurement for evaluating a material's ability to retain energy until it fractures (area under stress-strain curve)

^^

<b>under-reinforced section</b>	The ratio of reinforcement supplied in an under-reinforced section is smaller than that given in a balanced section.
<b>Uniaxial loading</b>	When all of the applied load are acting along the same axis
<b>yielding</b>	The yield phase is that phase at which a substance begins to bend plastically.

“

# Chapter 1: Introduction

..

## 1. Introduction

The serviceability of structural reinforcement can be compromised by many factors, including severe environments and incredibly high external loads. Corrosion in steel reinforcement is a significant contributor to structural deterioration. As a result, using noncorrosive insulation may be an effective way to prolong the operational life of RC systems. In the civil engineering field, the fibre polymer (FRP) bar is a novel and sustainable alternative to traditional steel reinforcement. The FRP composites consist of fibre-reinforced polymers; the fibres could be created from Glass, Carbon, Aramid, or Basalt. Each FRP type is characterized by different mechanical and physical properties and surface configurations. The FRP matrix usually is an epoxy resin that bonds fibres with the polymers. The use of FRP insulation will decrease potential maintenance and repair costs by preventing deterioration and, as a result, increasing the reliability and service life of concrete structures. FRP bars have many characteristics, including a lower weight/strength rate when compared to steel ( $1/5$  to  $1/4$  the steel density), superior tensile strength, and non-magnetic characteristics. The ductility of concrete members is affected by the linear elastic behaviour of Fiber-reinforced polymer (FRP) bars before failure initiation (brittleness).

Furthermore, the failure response of FRP reinforcement in concrete structures differs markedly from reinforcement quantity. The most common and used type of iron is Glass fibre; it is thought to become a better replacement for conventional steel rebar. Due to their lower elastic modulus, GFRP RC beams exhibit more considerable deflections and fracture widths when comparing to steel RC beams with the same reinforcement. It is also worth

..

noting that there is a specific code for FRP under the name: ACI440.1. This code provides instructions for the construction and implementation of concrete members reinforced with FRP. The ACI configuration merely mentions non-pre-stressed FRP reinforcement. It is based on experience obtained from global scientific research, empirical science, and field applications of FRP amplification.

The document guidelines of the ACI code are meant to be conservative. There are two types of failure modes in RC members; shear and flexural failure. The shear failure is sudden; it has the opportunity to have disastrous consequences. The flexural failure happens due to GFRP bar rupture if under-reinforced or by concrete crushing if over-reinforced. Two kinds of flexural faults can occur: a) Concrete crushing after GFRP rupture (under-reinforced section) b) Crushing of concrete before GFRP rupture (over-reinforced section). Comprehending the reaction of composite systems under loading is fundamental for modelling a cost-effective, efficient, and safe design. There are numerous theoretical, numerical, and computational techniques for modelling concrete systems.

Finite element (FE) analysis is a standard numerical approach for studying nonlinear material behaviour in concrete structures. The finite element analysis (FEA) algorithm is used to model and design the performance of strengthened and pre-stressed concrete components. There are various excellently FEA codes available, as well as customized components for complicated simulations. One of this FEA software is ANSYS. Because each material component has a complicated stress-strain behaviour, this nonlinear software is critical in the nonlinear response analysis. ANSYS has a 3-dimensional element (SOLID185) with nonlinear brittle materials comparable to concrete materials. Solid185 comprises eight nodes, while Reinf264 was used in ANSYS Software to simulate GFRP

..

bars and Stirrups of RC beams. This research reflects a substantial effort to efficiently utilizing ANSYS software to validate the experimental and theoretical (ACI 440.1) findings. The study also demonstrates how the conduct of RC beams with GFRP reinforcement was well simulated under incremental static load. The study's results have been graphically represented, including a load-deflection curve, a stress-strain curve, and so on.

### 1.1.Objectives

- 1- To establish a non-linear finite element design with ANSYS software to mimic the conduct of concrete beams strengthened ultimately by GFRP rebars and stirrups under four points pseudo-static bending experiment, the planned outcomes are:
  - a) Failure modes and cracking patterns.
  - b) Ultimate load and load-deflection slopes.
  - c) Stress-strain response of the GFRP rebar and concrete.
- 2- To verify the results from the virtual testing output of the FE model with the physical experimental outcome. The acceptable error for test verification is planned to be less than 10%.

..

## 1.2. Research significance and novelty

Steel is the most widely material that has been used in a civil structure as reinforcement for concrete. Despite the apparent advantages of steel, it has several limitations that make it unsuitable in some applications. One of these limitations is durability, as it is vulnerable to corrosion, especially in aggressive environments, resulting in costly retrofitting and maintenance. According to the issue mentioned above, GFRP is emerged to compete against steel. Unlike GFRP, steel is intensively studied, and its behaviour is well established. A comprehensive study of GFRP reinforcement in structural members is limited and needs to be emphasized. This research will help in comprehension of the flexural conduct of reinforcement of rectangular beams by GFRP rebar.

The conventional method to explore the mechanical properties of structural members is by conducting experimental work. This method is costly and time-consuming. On top of that, it is not environmentally friendly as it produces waste and consumes energy. One such solution is to virtually test specimens via the FE computer model. This research will establish a verified FE model to test and assess the flexural conduct of reinforced concrete beams with GFRP rebar. The model will help test many specimens by altering key variables to take full advantage of this composite system which will undoubtedly benefit this research field. Research that undertook the FEA as a testing method is minimal when compared with actual experiment testing. FEA of such a composite system is the novelty of this study.

“

## Chapter 2: Literature Review

## 2. Chapter 2: Literature Review

### 2.1. Durability

Nowadays, with the spread and increase in the uses and applications of FRP in the field of civil engineering, significantly as reinforcing in concrete structures, the interest of many engineers and researchers has increased in understanding and studying the durability of FRP material which in turn explains what the state of the material will be. And its effectiveness in the long term [1]. Studying and understanding the durability of FRP is crucial with its tremendous spread and use in civil engineering applications. FRP is a relatively new material with a limited track record. Therefore, quality control, performance, and long-term usability, durability must be deeply investigated. This section will focus on reviewing the recent study on the durability of FRP as concrete reinforcement.

Paul Boer et al. [2] thoroughly reviewed the environmental effects on the durability of FRP. Inclusive, the review found that FRP is variable to moisture as the risen will be affected by absorption. The risen degradation could be reduced markedly if the risen is allowed to cure before exposure completely. Moreover, the coating can prevent moisture absorption as well as rust prevention. The review also points toward the negative effect of the alkaline solution in pure concrete water on FRP. It speeds up the deterioration of the bond between the risen fibres. The thermal impact does affect the durability of such materials. A moderate increase in temperature could help cure the composite. Still, a high rise in temperature will be detrimental to the risen and the adhesive. It leads to a loss in the elastic mechanical properties and increases its variability to moisture absorption.

Meanwhile, frigid temperature could cause to hardening effect to the matrix and micro-cracking, and fibre-matrix deterioration. The authors noted that the freezing and thawing cycle is the most worrisome threat to FRP. It generates delamination that could speed the

..

deterioration due to expansion and salt penetration into the matrix. Careful consideration should be taken toward the coefficient of thermal expansion to evade premature failure. Moreover, allowing the resin to cure fully is crucial to prevent creeping behavior and relaxation issues. Unlike the fibres in FRP, the matrix is combustible, and, when exposed to fire or extremely high temperature, catastrophic failure could ensue.

Two main tests are implemented to evaluate the durability of concrete structures reinforced with FRP, namely, the natural ageing test and the accelerated ageing test [3, 4]. Although natural ageing testing is time-consuming, the experimental results are far more reliable and simulate reality because it suffers from environmental influences experienced in daily life. Accelerated ageing test accelerates the impacts to components by growing the degree of exposure to severe environments to know and interpret the durability of the member within a short period [5, 6].

Regarding the durability test of the GFRP bars, in 2007, Mufti et al. [7] examined the durability of GFRP rebars by testing five GFRP reinforced concrete bridges that were used from 5 to 8 years. During that time, both Fourier transform electron microscopy (SEM), and infrared spectrum (FTIR) were used, and the glass transition temperature ( $T_g$ ). Overall, the results found from the tests did not show any apparent differences or deterioration in GFRP reinforcement's strength.

Li Shan. et al. [8] conducted a test on CFRP and GFRP samples, where he exposed these samples to different temperatures (30, 40, 50, 60°C) and put them in an alkaline solution to a static tensile test. The findings of the tests showed a gradual decline in tensile strength, modulus of elasticity, CFRP and GFRP elongation increasing ageing time. It was also observed that with increasing temperature, the rate of these properties increased.

..

Early research on durability suggests that for GFRP bars, concrete pore solutions are an offensive setting. [9-13]. This, in turn, may contribute to fibreglass damage or the dissolution of the sides between the resin and the fibre. Moreover, the infrastructure is exposed to many external factors throughout its service life, which leads to a deterioration in the properties of the materials [14] and the bonding of bars of GFRP inside the concrete [15].

Recently, researchers have shown increasing interest in studying certain types of environments such as high humidity, salty and alkaline environments. They cause the vast majority of problems in reinforced concrete elements [16]. The mechanical properties of the reinforcing material are often utilized to assess the durability of the reinforcing material as a result of accelerated testing and program evaluation methods through the use of GFRP bars [17].

Through an experiment carried out by Kim et al. [18], he put GFRP bars in various chemical solutions at room temperature and high temperatures to hasten the deterioration procedure. The test outcome showed the effect of alkaline solutions on the FRP bars, as the tensile strength of the FRP rebar was decreased by 60% after 132 days for electronic glass/vinyl ester.

..

## 2.2. Bond Strength

Steel reinforcement is vulnerable to an aggressive environment. For such reasons, alternatives have been sought by engineers and researchers. One such alternative is the fibres reinforced polymer reinforcement (FRP) bars. FRP has many advantages that could be exploited in many applications: high strength/weight ratio, handling ease, and nature of electromagnetic [19]. Additionally, it is not influenced by electrochemical corrosion [20-22].

Despite obvious benefits, FRP has some limitations in toughness and bond strength with reinforced concrete when compared to conventional reinforcement bars. [23]. Over the last few years, the bond strength of GFRP and concrete was already extensively investigated. Many studies have shown how the bond strength of GFRP reinforcement rebar is noticeably lesser than that of comparable strength steel bars.[24-26].

Ivan Holly et al. [26, 27] presented an assessment of the bond conduct of GFRP rebar and steel models because the steel rebar models provide reliable findings for determining the bond conduct of GFRP bars models. The faces of the interconnected surfaces between concrete and GFRP rebar are entirely dissimilar from the bond surfaces of steel bars and concrete. That is because of the availability of many GFRP rebar commercially with numerous composites and various surface treatments. They have reported that the bond conduct for both deformed surface and straight smooth surface of FRP rebar are affected by many factors such as the confinement pressure of FRP rebar, the diameter of rebar, influence of the position of the bar in casting, influence of top-bar, the length of embedment, the condition of the environment, and the changing in temperature [28].

..

Natalia et al. [29] conducted pull-out experiments on cubes of GFRP reinforced concrete. They stated how the GFRP and concrete's bonding strength is strictly dependent on the shear resistance among successive layers of fibers and rebar deformation. Moreover, the curing time and method effectively provide sufficient concrete confinement of the reinforcement surface failure and the link with both binding the stress and GFRP reinforcement slippage.

As a comparison, D. Szczech et al. [30] evaluated the strength of the bond of GFRP bars with concrete to steel bond with concrete as a benchmark. They have 18 reinforced beam bond specimens aiming to measure the impact of a different variable on bond strength. The rebar diameter (12, 16, 18 mm) and type of reinforcement were used as measuring parameters (sand-coated GFRP and steel). The researchers discovered how the rebar bond strength with 16 and 18mm diameter of GFRP reinforced concrete is slightly weaker than steel but that the bond strength of 12mm GFRP rebars is greater than steel-reinforced concrete.

Two different experiments are utilizing to compute the reinforcing bars bond strength: pull-out and beam tests [31]. The results that were obtained from each test could vary. The results gained from pull-out tests are usually higher than those from the beam tests. This is caused by averting concrete splitting in the pull-out tests. This is due to several reasons: the non-existent local bending resistance, the higher concrete cover, and the concrete sample.

Meanwhile, in the beam test, the underlying concrete stresses the concrete are tension and vary along the beam's span. Accordingly, the performance of bond-slip of FRP rebar will be higher in pull-out tests than beam tests. Therefore, when concrete members' actual

..

conduct needs to simulate flexure, the pull-out tests are less realistic than the beam tests, which some researchers have said. The Pull-out test is the simplest and thus the most widely used by researchers.

Many troubles can be faced during maintaining an ageing concrete structure, such as corrosion of steel rebar correlating with spalling and cracking in concrete covers [22, 32-35]. GFRP rebar has various material characteristics than steel rebar. Due to the manufacturing procedure of GFRP rebar, it is considered an ingrained orthotropic material, while steel rebar had isotropic properties [33, 36]. According to recent research, concrete and GFRP rebar bonds are weaker than steel rebar [22, 34, 37-40]. It was noted that the GFRP rebar bond strength is approximately 60 per cent less than that of the corresponding strength rebar of steel [40-42].

The difference in the strength of bond among GFRP and steel rebar can be attributed to the nature of the deformed steel reinforcing surface with its ribs which in turn contributes to the On the other hand, and there are several methods of surface treatment [40, 43], including sand coatings and spiral formations. Using and developing these methods, the surfaces of GFRP rebar become rough and deformed, raising the bond strength to the required extent. The deformed steel rebar has been compared with three types of FRP rebar with different surfaces under sustained loads in terms of long-term bond behaviour [44-46].

Each type of FRP has been different surface; for example, the surface arrangement of type A was sanding coating with lugs wrapped in a double helical pattern of GFRP, while the surface configuration of type B was serrated in the form of a double helical pattern. Type

..

C surface was consisting of seven smooth strands of twisted cable. It has been found that the surface arrangement significantly influenced the bonding strength of FRP rebar. The best type of FRP was type B; It presented the most significant bond strength. Despite that, all three different types of surfaces of FRP were showed less bond capacity comparing with rebar of steel. The pull-out tests that utilized to assess the conduct of FRP rebar bonds. [40].

There are a variety of surface treatments that can be used to enhance bond strength. As compared to other surface treatment approaches, the deformed surface approach gave the highest bond efficiency. It was found that the use of square cross-section bars increases the bonding between concrete and GFRP rebar, and it was observed that the bonding strength of square bars around 25 per cent more than those of round rebar due to the influence of wedging [47]. Many different forms and substances of macro fibers have been supplementary to the concrete matrix to increase the bond's capacity among GFRP rebar and concrete. [37].

Two sorts of macro fibers have been used, PPA fibres and steel fibres, to improve FRP and concrete bonds. The pull-out test examined steel rebar samples and GFRP rebar samples. By adding 30 Kg/m<sup>3</sup> steel fibres and 2 kg/m<sup>3</sup> PPA fibres to concrete, the bond strength will reach a maximum between concrete and GFRP rebar. Despite enhancements and increased bond strength of concrete and GFRP rebar, the bonding strength is even less than that found between steel rebar and normal concrete without fibres. It was discovered that the confinement pressure of GFRP rebar affected the bond strength among GFRP rebar and concrete. [35, 48-50].

..

Laboratory experiments have been performed to examine the impact of GFRP rebar confinement pressure on the strength of bonds among concrete and GFRP rebar. Four different kinds of GFRP bars with other surfaces have been used during the experiment. Type A is a deformed surface that looks like steel rebar, type B is a rough surface, and type C and type D were smooth strands twist several. Each type of rebar was applied confinement pressure on it with different MPa pressure. By performing the pull-out test on the GFRP rebar, the results illustrate that, by applied confinement pressure on rebar, the bond strength of the GFRP rebar and concrete will increase and will achieve the highest bond strength by rebar with a deformed surface (type A) and a confinement pressure of 24.1 MPa [50].

Another method for applying confinement pressure to the GFRP rebar has been used. This method used three different batch samples. The first samples were steel bars with normal concrete. The second samples were GFRP rebar with the sand coating with normal concrete. The third samples were GFRP rebar with expansive concrete. In normal concrete, the bond strength of steel rebar was discovered to be greater than that of GFRP rebar. The GFRP rebar bond strength surrounded in expansive concrete and adjusted by CSA Calcium sulfoaluminate was improved to reach similar as the steel bars bond strength in normal concrete or more significant than it [51].

We should consider the critical issue to ensure the composite of GFRP and concrete are joined and worked very well is the bond between them. Many factors affect GFRP bars and concrete bonds, such as Adhesive chemicals, friction, and friction between rough bar surfaces with practical broken concrete [52].

..

GFRP rebar has many properties that make it the best alternative to steel rebar. On the other hand, GFRP rebar has disadvantages. One of these disadvantages is its weak bond with the surrounding concrete [20, 46, 48, 53, 54]. Completely unlike steel, GFRP rebars elastic modulus and surface profiling are lower than steel; besides, the effect of interlocking is reduced as well [55].

Commonly, the GFRP rebar showed pretty bond conduct in the whole of the examined study.

The ultimate bonding strength of FRP rebar and concrete is somewhat like those of steel and concrete. The similarity ratio between the two is close to 85 per cent [56]. Many parameters can affect FRP bond conditions, such as concrete strength and modulus of elasticity for FRP rebar. Still, the most influential parameter, which is a crucial parameter, is the surface preparation of FRP rebar. Also, although the rod diameter is the same, FRP rebar has a lesser bond strength to concrete than steel rebar. This could be due to the ribs since the majority of GFRP rebar are ostensibly clipped from the core.

..

### 2.3. Shear and Flexural Strength

As a concrete structural reinforcement, fiber-reinforced polymer (FRP) rebar varies significantly from steel reinforcing bars. Mainly, FRP materials are linearly elastic up to failure, while steel yields at higher stresses. Since both the concrete and the FRP rebars have a brittle failure, the structural member will fail suddenly without sufficient warning, resulting in a catastrophic failure of the member. To tackle the issue mentioned earlier, the ACI 440.R1 guideline [57] recommends reinforcing the structural members against both shear and flexural to invoke concrete failure before reinforcement failure. This section presents a literature review of the development of GFRP rebars as shear and flexural reinforcement.

Furthermore, FRP is linearly elastic until failure, leading to brittle failure without adequate warning. Glass fibre reinforced polymer (GFRP) has much usually had far less elastic modulus value when compared to steel. This could result in insufficient ductility of structure and serviceability due to cracking and deformation in members of concrete reinforced by FRP.

By the 2000s, many provisions and standards were developed for the user community to deliver shear design methods and guidance for structural concrete reinforced by FRP reinforcement. Among them is the American Concrete Institute. (ACI 440.1-R06) [57] the procedure, the American Association of Highway and Transportation officials (AASHTO) [58], Japan society of civil and Engineering (JSCE 1997) [59], the Canadian Standard Association (CSA S6-06) [60], and the Italian Research council CNR DT-203/2006. Each

..

guideline is different in terms of the contribution of FRP stirrups and concrete in shear capacity.

Nagaska et al. [61] have identified and classified the shear failures of GFRP stirrup-reinforced beams into two types; those are shear tension failure which occurs when the FRP stirrups fractures after reaching its ultimate strain capacity, and secondly, shear compression failure as a result of the crushing of concrete web. They have also confirmed that shear failure is more desirable as it is less brittle. The reinforcement ratio of the members entirely defines the mode of failure.

In Japan, Machida et al. [62] conducted one of the earliest experiments of beams reinforced with GFRP rebars. They have recommended using a higher safety factor in design than steel reinforcement to avoid brittle failures and guarantee the reinforcement of the member. Shortly, the Japanese design code incorporated his recommendation for designing a concrete element with FRP reinforcement.

Nawi et al. [63] evaluated the influence of reinforcement ratio on reinforced concrete beams with GFRP and steel bars as a comparison. They have established that the reinforcement ratio beyond the balanced reinforcement ratio of the member will not significantly affect the beams carrying capacity. The beam failure would be governed by concrete crushing in the compression region in an instance of flexural failure or concrete shear failure in an instance of shear failure.

Habib et al. [64] tested the shear and flexural capacity of reinforced concrete members of GFRP bars in the presence of points loading. Those beams were exclusively reinforced in tension and shear without compression reinforcement. The experimental variables were

..

compressive strength, reinforcement ratio, and the beam's depth. As a result, two different failures were obtained: the concrete shear failure in concrete span and flexural failure in the compression region. The authors have also gained a post-cracking stiffness factor for those beams in Branson's equation.

Tottori et al. [65] investigated the shear capacity of members reinforced with Glass FRP, carbon FRP, and Vinyon FRP stirrups. The authors reported that the shear capacity contributed by the concrete compression region and the aggregate interlock was linked to the tensile strength and stiffness of the longitudinal FRP reinforcement. Moreover, the contribution of concrete and the FRP in shear resistance were similar.

Joseph R. Yost et al. [66] presented experimental data of 21 beams regarding the shear and flexural strength of rectangular beams of GFRP reinforcement rebar. The beams had not been reinforced with shear stirrups and considered the primary variable as the longitudinal reinforcement. e out of the 21 beams were reinforced with steel rebar for test control, and the remaining were reinforced by GFRP rebar. The beams had been examined in a mid-shear span to an adequate depth  $\left(\frac{a}{d}\right)$  ratio of around 4.0. They found that the total number of longitudinal reinforcement had no considerable impact on the shear capacity of the members. Moreover, the characteristics of the concrete shear failure of those beams were very similar to traditional beams. The ACI 318 [67] equation of shear strength is not conservative and for beams with FRP reinforcement.

In 2015, an article published by Juoza Valivonis et al. [68] aiming to study experimentally the rectangular beams shear resistance reinforced by fibre-reinforced polymer stirrups along with the theoretical provisions from the literature. Their experimental program

..

involved testing four doubly reinforced rectangular beams and investigating the shear response of the experimental results and 102 beams from the database from the literature. It compared it with the available provision and proposed an analytical model for designing such beams. They have claimed that the available analytical models are intended to calculate the shear-resistant reinforced beams with steel and are not recommended for FRP reinforced beams.

Another experimental program was conducted by Emile Shehata [69] to assess the structural performance of FRP stirrups as shear reinforcement of concrete members. They have examined a total of 10 large-scale GFRP reinforced concrete beams to measure the impact of FRP stirrups and concrete on the shear carrying capacity and compared it with beams reinforced with steel for test control. The testing variables were the stirrups spacing and the reinforcement (GFRP and steel). Because of the unidirectional properties of GFRP, a noticeable decrease in strength of the stirrups relative to the tensile strength of the fibres is induced by bending the FRP rebar into a stirrup formation. The authors reported that the concrete contribution in shear capacity is less than the FRP stirrups compared to traditional reinforcement. Moreover, they have recommended a minimum shear reinforcement ratio to ensure that shear strength outstrips cracking load.

M. Talha et al. [70-73] tested 48 (GFRP) glass fiber reinforce polymer beams to study the effect of distinct concrete types on the flexural behaviour and deflection. That concrete was Ordinary Portland-based concrete, fibre reinforced concrete (with discrete fibres), Geopolymer concrete (GPC), and fibre-reinforced geopolymer concrete (FRGC). The authors reported that the deformed surface GFRP bars are suitable for internal

..

reinforcement for the four different types of concrete. However, careful attention should be given to the various properties of the concrete used.

## 2.4.Design philosophy

### 2.4.1. Flexural Design

Based on previous studies [74, 75], it has been found that the flexural design method for concrete with GFRP reinforcement is similar to concrete with steel reinforcement. By referring to the laboratory data, it is concluded that the flexural capacity calculations of concrete members reinforced with FRP be able to be expected by calculating the flexural capacity of steel rods because of their similarity. When designing concrete members with FRP reinforcement, attention should be paid to the stress and strain of the FRP materials' uniaxial relationship. The philosophy of Flexural design of steel-reinforced concrete members aims to ensure steel yield before the concrete is crushed. The importance of the yield in steel is to give it ductility, which makes it deformed before fracturing, issuing a warning before failure occurs.

On the other hand, unlike steel, FRP material does not have ductility; it is a brittle material that leads to failure directly without warning, requiring a reconsideration for use.

If the FRP reinforced concrete member ruptures, failure occurs suddenly and without warning [74, 76].

The significant elongation in the FRP reinforcement creates a large deformation that gives a slight warning before rupture.

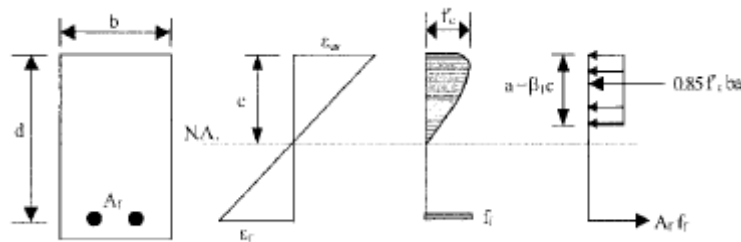
..

ACI-440R1-06 [77] states that the factored moment capacity to be higher than the ultimate moment capacity as the following equation:

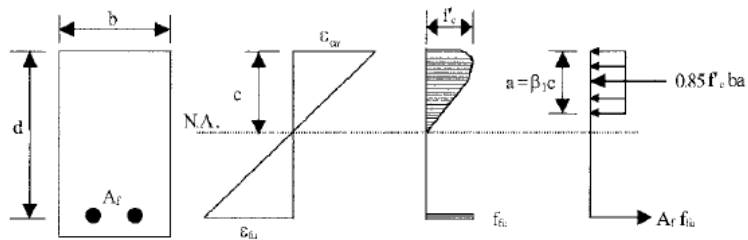
$$\phi M_n \geq M_u \quad (1)$$

Compatibility of strain, an equilibrium of internal force, and the failure controlling mode, all of these things, we can specify the nominal flexural strength of concrete member reinforced by FRP.

Figure 1 below illustrates the three different cases of stress, strain, and internal forces of FRP-reinforced rectangular section.

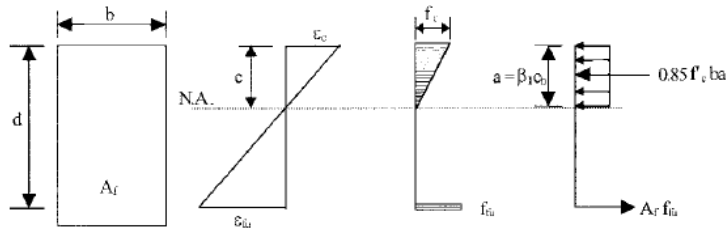


a) The failure occurred due to the concrete crushing



b) Failure equilibrium condition

..



c) The failure occurred due to FRP rupture

Figure 1: Distribution of strain and stress under ultimate instances.[77]

Two different kinds of flexural capacity failure may arise in concrete components reinforced with FRP: crushing of concrete or rupture of FRP. By evaluating the proportion of FRP reinforcement to balanced reinforcement (The ratio that both types of failure coincide), the failure mode can be specified. The balanced reinforcement ratio of FRP is calculated by utilizing the tensile strength design because the FRP is not approach yielded behaviour.

The below equations show that: a) calculation the ratio of FRP reinforcement b) calculation the ratio of balanced FRP reinforcement:

a) FRP reinforcement ratio:  $\rho_f = \frac{A_f}{bd}$  (2)

b) Balanced FRP reinforcement ratio:  $\rho_{fb} = 0.85 \beta_1 \frac{f'_c}{f_{fu}} \frac{E_f \epsilon_{cu}}{E_f \epsilon_{cu} + f_{fu}}$  (3)

The criterion for determining the type of failure mode is calculating the rho value; if the rho of reinforcement ratio was lesser than the rho of balanced reinforcement ratio, the mode of failure that occurred was FRP rupture failure. In contrast, if the value of rho is more significant than the rho of balanced ratio, the failure mode was concrete crushing.

..

**Calculations of the nominal flexural strength** will be different based on the mode of failure.

If the  $\rho_f > \rho_{fb}$ , that is mean the failure mode is concrete crushing. Depend on the consistency of strain and the equilibrium of forces. The following symbols can be derived:

$$a) M_n = A_f f_f \left( d - \frac{a}{2} \right) \quad (4)$$

$$b) a = \left( \frac{A_f f_f}{0.85 f_{cb}} \right) \quad (5)$$

$$c) f_t = E_f \varepsilon_{cu} \frac{\beta_1 d - a}{a} \quad (6)$$

*By substituting the above equations, we can find a value of  $f_f$*

$$f_f = \left( \sqrt{\frac{(E_f \varepsilon_{cu})^2}{4} + \frac{0.85 \beta_1 f_{c'}}{\rho_f} E_f \varepsilon_{cu}} - 0.5 E_f \varepsilon_{cu} \right) \leq f_{fu} \quad (7)$$

*The nominal flexural strength could be represented by changing the equation above by*

$$M_n = \rho_f f_f \left( 1 - 0.59 \frac{\rho_f f_f}{f_{c'}} \right) b d^2 \quad (8)$$

While when the  $\rho_f < \rho_{fb}$ , that is mean the failure mode is FRP rupture bar. The ACI stress block in this type of failure is not valid. Because the max strain value of concrete 0.003 may not be achieved. The nominal flexural strength in this failure mode can be estimated using the following formula:

$$M_n = A_f f_{fu} \left( d - \frac{\beta_1 c}{2} \right) \quad (9)$$

The maximum multiplication value can obtain  $\beta_1 c b$ . It can be achieved when the strain of concrete reaches the maximum (0.003). The following equations illustrate that:

..

$$Mn = A_f f_{fu} \left( d - \frac{\beta_1 c b}{2} \right) \quad (10)$$

$$Cb = \left( \frac{\varepsilon_{cu}}{\varepsilon_{cu} + \varepsilon_{fu}} \right) d \quad (11)$$

The nature of FRP members behave in a non-ductile behaviour, so the strength reduction factor must be used in the calculations to achieve a greater level of reserve strength in the member. Japanese researchers have recommended using the strength reduction factor equal to 0.77 for design flexural member's purposes [59]. At the same time, other researchers recommended, based on probabilistic concepts, a value of 0.75 (strength reduction factor) for flexural design. Likewise, the ACI code recommends using 0.65 of the factor for compression controlled failure for design purposes.

The equations used to calculate the strength reduction factor for flexural design are shown below:

$$\phi = \begin{cases} 0.55 & \text{for } \rho_f \leq \rho_{fb} \\ 0.3 + 0.25 \frac{\rho_f}{\rho_{fb}} & \text{for } \rho_{fb} < \rho_f < 1.4\rho_{fb} \\ 0.65 & \text{for } \rho_f \geq 1.4\rho_{fb} \end{cases} \quad (12)$$

The equations are illustrated and also presented graphically as shown in the Figure 2 below:

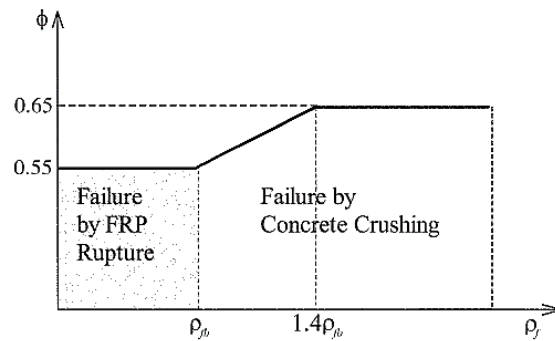


Figure 2: The strength reducing factor as a function of reinforcement proportion [77].

..

Returning to the equations and the graph, it can be concluded that the coefficient with a value of 0.65 represents sections controlled for concrete crushing. In contrast, the coefficient with a value of 0.55 is a coefficient that returns to the FRP ruptured sections and makes a linear link among them.

**The minimum reinforcement of FRP** Minimum reinforcement should be provided when designing the failed member due to the rupture of FRP  $\rho_f < \rho_{fb}$ , which will prevent concrete cracking failure (that is,  $\phi M_n \geq M_{cr}$ ) as well.

The minimum reinforcement area of FRP members can be calculated by multiplying the rebar formula obtained from the ACI code 318-05 [67] by the value 1.64. This will be illustrated in the following equation:

$$A_{f, \min} = \frac{4.9 \sqrt{f_c}}{f_{fu}} b_w d \geq \frac{330}{f_{fu}} b_w d \quad (13)$$

The minimum reinforcement to prevent cracking in the concrete is automatically achieved if the FRP rupture of  $\rho_f$  does not control the member failure  $> \rho_{fb}$ .

If  $\rho_f < \rho_{fb}$ . The equation  $A_{f, \min} = \frac{4.9 \sqrt{f_c}}{f_{fu}} b_w d \geq \frac{330}{f_{fu}} b_w d$  is required to check.

..

### 2.4.2. Shear Design

A remarkable similarity in design between concrete members reinforced with steel and concrete members reinforced with FRP. Their mechanical properties distinguish steel rebar. However, the shear must be considered. When designing the shear of FRP reinforced concrete members, some points must be taken care of, is as follows:

- The FRP modulus of elasticity is relatively low.
- The transverse shear resistance of the FRP is low.
- FRP has high tensile strength while not having a yield point. Besides, the strength of the straight FRP rebar is much higher than that of the bent FRP rebar.

The strength design method is the basis upon which to design the shear for FRP reinforcement depends. For reducing the nominal shear capacity of FRP reinforcement, it should take as strength reduction factor used for steel-reinforced concrete members, which are 0.75, and it was taken from ACI 318-05 [67] code. The factored shear strength value  $\phi V_n$  should be higher than the factored shear force value  $V_u$ . Using the ACI 318-05 [67] code can calculate the maximum shear force at supports of the beam.

As indicated by [67] ACI 318-05, The amount of shear resistance delivered by concrete  $V_c$  and shear reinforcement of steel  $V_s$  determines the nominal shear strength of a reinforced concrete cross-section  $V_n$ .

Compared to a steel-reinforced element with equivalent longitudinal reinforcement parts, a cross-segment utilizing flexural reinforcement of FRP, after cracking, has a lower depth to the neutral axis due to the decreased axial stiffness. The cross-sectional compression area has diminished, and the crack widths have increased. As a consequence, the shear

..

resistance given by aggregate interlock and compressed concrete is more minor. According to a study on the flexural shear capability of members without shear reinforcement, the tensile (flexural) reinforcement stiffness influences concrete shear strength. [61, 78-82].

The contribution of the longitudinal strengthening of the FRP Terms of Dowel Action has not been set. Since FRP bars have lower transverse strength and stiffness, This is presumed that their dowel action contribution is much lower than that of a corresponding steel part.

The following equation can be utilized to calculate the concrete shear capacity  $V_c$  for flexural FRP reinforced members as the main reinforcement:

$$V_c = 5\sqrt{f'_c} b_w c \quad (14)$$

For SI units

$$V_c = \frac{2}{5}\sqrt{f'_c} b_w c \quad (14)$$

Where;  $b_w$  = web width and  $c$  = cracked transformed section neutral axis depth Term “c” (neutral axis depth) can be calculated for rectangular cross-section with singly reinforced as following:

$$c=kd \quad (15)$$

$$k=\sqrt{2\rho_f n_f + (\rho_f n_f)^2} - \rho_f n_f \quad (16)$$

$$\rho_f = \text{FRP reinforcement ratio} = \frac{A_f}{b_w d} \quad (17)$$

The following formula can be utilized to reform the equation for the shear capacity of concrete  $V_c$  of flexural members:

..

$$V_c = \left(\frac{2}{5}k\right)2\sqrt{f'_c} b_w d \quad (18)$$

The ACI 318-05 [67] methodology used for the shear measurement of the contribution of steel stirrups is viable to the application when FRP is used as shear reinforcement. The shear resistance is given by FRP stirrups orthogonal to the member Vf axis be able to compute as seen below:

$$V_f = \frac{A_{fv}f_{fv}d}{s} \quad (19)$$

the below equation offers the ultimate stress level of FRP shear reinforcement to be used in the design:

$$f_{fv} = 0.004E_f \leq f_{fb} \quad (20)$$

The required spacing and shear reinforcement area for shear reinforcement perpendicular to the axis of the member be able to be determined using the below formula:

$$\frac{A_{fv}}{s} = \frac{(V_u - \phi V_c)}{\phi f_{fv} d} \quad (21)$$

When the shear reinforcement is used with inclined FRP stirrups, the equation below is used to measure the FRP stirrup contribution.

$$V_f = \frac{A_{fv}f_{fv}d}{s} (\sin \alpha + \cos \alpha) \quad (22)$$

..

When the rectangular spirals of continuous FRP are utilized as shear reinforcement (in this status, the pitch is  $s$ , and the alpha is the Inclination angle of the spiral), the equation below contributes to the spirals of the spiral FRP.

$$V_f = \frac{A_{fv} f_{fv} d}{s} (\sin \alpha) \quad (23)$$

Shear failure modes are classified into two types for FRP members used as shear reinforcement [61]: shear-tension failure mode (managed by FRP rupture) and shear-compression mode failure (managed by the crushing web). The more brittle is the first mode, and the second produces the most considerable deflections.

To compute the minimum shear reinforcement of FRP, the following equation offers that:

$$A_{fv,min} = \frac{50b_w s}{f_{fv}} \quad (25)$$

For SI units

$$A_{fv,min} = 0.35 \frac{b_w s}{f_{fv}} \quad (25)$$

..

## 2.5. Design Applications

A significant study has been carried out on developments of FRP composite materials and their groundbreaking applications. FRP composite is marketed as 21st-century materials owing to perfect corrosion resistance, perfect thermomechanical properties, and great strength to weight proportion. In civil and military infrastructures, the use of FRP composite will enhance creativity, enhance productivity, increase performance, and have a longer service life, i.e., decreased lifecycle costs. There is considerable scope for using innovative composite materials and design to minimize the weakness of infrastructure.

When constructing particular structures, consideration must be given to the properties of the FRP reinforcement to evaluate if it is appropriate or essential.

The FRP corrosion resistance is a substantial advantage to structures in an extremely aggressive environment; for instance, dams and additional marine structures, bridges, and superstructures are often exposed to dissolving salt and handling with deicing salts. Although FRP reinforcement has brittle behaviour, the high strength of FRP compensates for this. FRP reinforcement must primarily be employed in systems that benefit considerably from several qualities properties, like nonconductive or noncorrosive characteristics of their materials. FRP reinforcement for moment frames or regions that moment redistribution is mandatory is not suggested caused by a shortage of knowledge in its application. Relying on FRP reinforcement to withstand compression is insufficient. Because of the combined effect of that kind of action and the markedly decreased FRP modulus compared to steel, the calculation of extreme assistance at the concrete crushing of compression of FRP reinforcement is small.[77]

..

## 2.6. ACI Formulation

The FE model is also compared with the ACI guideline for the mid-span deflection calculation. The following steps are followed accordingly. With the given geometry of the specimen (h, b, d), the beam section gross moment of inertia  $I_g$  can be calculated as follow:

$$I_g = \frac{bh^3}{12} \quad (26)$$

Then, using the below formula, the proportion of FRP modulus of elasticity to the concrete modulus of elasticity "nf" is computed.:

$$n_f = \frac{E_f}{E_c} = \frac{E_f}{4750\sqrt{f'_c}} \quad (27)$$

Subsequently, the "K" factor is computed using the given formula:

$$K = \sqrt{2\rho_f n_f + (\rho_f n_f)^2} - \rho_f n_f \quad (28)$$

The moment of inertia of the transformed cracked section of the beam "I<sub>cr</sub>" will then be computed using the equation below:

$$I_{cr} = \frac{bd^3}{3} K^3 + n_f A_f d^2 (1 - K)^2 \quad (29)$$

The stress in FRP rebars may also be computed using the following formula:

$$f_r = 0.62\sqrt{f'_c} \quad (30)$$

The equation of cracking moment is:

$$M_{cr} = \frac{2f_r I_g}{h} \quad (31)$$

..

The formula of reduction factor which was used in the calculation of deflection " $\beta_d$ " has to illustrate below:

$$\beta_d = \frac{1}{5} \left[ \frac{\rho_f}{\rho_{fb}} \right] \quad (32)$$

The equation can calculate the deflection due to applied load:

$$(I_e) = \left( \frac{M_{cr}}{M_a} \right)^3 \beta_d I_g + \left[ 1 - \left( \frac{M_{cr}}{M_a} \right)^3 \right] I_{cr} \quad (33)$$

$$(\Delta_i) = \frac{5Ml^2}{48E_c(I_e)} \quad (34)$$

..

## 2.7. Finite Element

Premalatha, J. et al. [83] implemented a nonlinear finite element analysis to mimic the actions of steel-reinforced concrete beams, and GFRP reinforced concrete beams. ANSYS program has been used for FEA. Four beams were modelled as control beams utilizing ANSYS software. Two beams of concrete have been used, one including steel reinforcement and the other with GFRP reinforcement. The other two beams with a mix of GFRP and Steel reinforcement have been utilized in concrete beams by varying the reinforcement percentage. Load-deflection and flexural capacity collected via the ANSYS software are consistent with experimental outcomes obtained by Wenjun et al. [84]. Failure of concrete beams reinforced with GFRP in the ultimate load region due to crushing concrete in the compression region. The accuracy of simulation between the FEA and experimental results at ultimate load is within 10%.

T. Subramani1 et al. [85] Created a Finite Element Model for a 3.0 m concrete beam reinforced with mild steel by ANSYS software to simulate an investigation done by Ayman and Banerjee [86]. The dedicated concrete components appropriately captured the nonlinear flexural response of the structures until failure. While using the finite element technique to estimate the intensity of actual beams, assigning suitable material properties is essential. They have confirmed that ANSYS is a time- and cost-effective modelling system that produces reliable findings.

Xingzhong Zhang et al. [87] Used ANSYS software to model a concrete beam reinforced with steel. The data gained by the ANSYS program was validated with the experimental findings. The observations illustrate how the ANSYS model results are similar to and

..

comparable to the experimental evidence results. As a result, it demonstrates the ANSYS program's ability to mimic the mechanical properties of concrete structures.

G. Vasudevan and colleagues [88]. Conducted analysis for six steel reinforced concrete beams exposed to four-point bending. The study compares the findings of experimental, analytical, and FEA. The ANSYS software was utilized to form the Finite Element model, and the computational equations for the analytical data were obtained from the IS 456: 200 code. The ANSYS software outputs, such as load and deflection patterns and stress-strain curvature, provide a more extensive view of the nonlinear conduct of reinforced concrete structures. IS 456: 2000 concrete material characteristics specifications will provide non-linear finite element analysis using the ANSYS software, and the outcomes were very close to the findings of experimental experimentation. The initial cracking conduct manner produced using IS 456: 2000, FEA, and analytical formulas are too tight. Depending on a broad set of simulations performed on RC beams utilizing ANSYS software, some results, such as deflection and rebar strain, were discovered to be more responsive to mesh size, material properties, load increments, and other variables at the final stage. The analytical ultimate moment potential derived by IS 456: 2000 is somewhat smaller than the experimental and finite element analysis estimations.

“

## Chapter 3: Finite Elements Modeling

### 3. Chapter 3: Finite Elements Modeling

The present study establishes a theoretical model of rectangular beams reinforced with GFRP rebars with ANSYS software.

#### 3.1. Case study

For academic purposes and to evaluate the work and the results obtained from the ANSYS program, the dimensions and characteristics of beams and the results of the test were taken from the laboratory study carried out by the researcher Abdalla Elbana et al. [70, 72, 73, 89-91] as a reference for comparison and evaluation. In this study, the researcher prepares concrete beam samples with GFRP reinforcement to evaluate the flexural behavior of the beams. The beams dimensions are illustrated in the Table 1:

Table 1: Beam properties that have been tested

Beam No.	h (mm)	b (mm)	a (mm)	L (mm)	Reinforcement
1	300	200	30	2400	Over –reinforced

All beam samples in the test have identical reinforcement, as all GFRP bars are used as main reinforcement in beam samples. Relative to flexural strength, rebar 2#16mm was used, where it was Over-reinforced to guarantee the occurrence of crushing of the concrete. The researcher used #10@70mm for the shear reinforcement, which is considered a heavy reinforcement to avoid shear failure.

..

In the compression zone, 2#10 mm diameter rebars were placed as hangers. There were no stirrups or compression reinforcement in the constant moment zone to prevent the strain and crack growth in the pure bending region.

The [Figure 3](#) below illustrates the arrangement of the main reinforcement and the stirrups of the GFRP rebar:

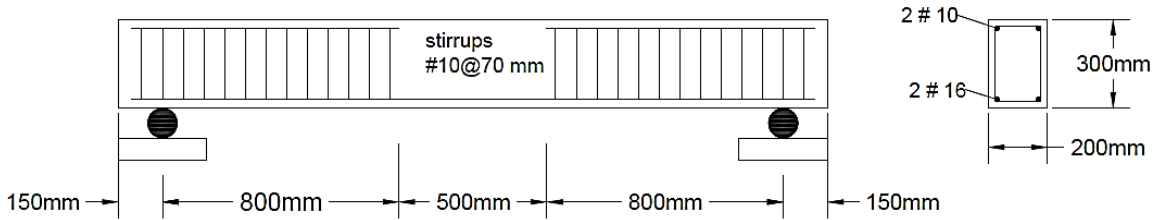


Figure 3: Reinforcement details of the tested beam

..

### 3.2. Test Set up

In this experiment, the flexural behavior of each beam sample was examined through four-point bending static test. All beams tested are simply supported beams, and a load with the rate of 0.01 mm/sec is applied to them gradually until the failure point. The [Figure 4](#) and [Figure 5](#) below demonstrates the features of the test machine:

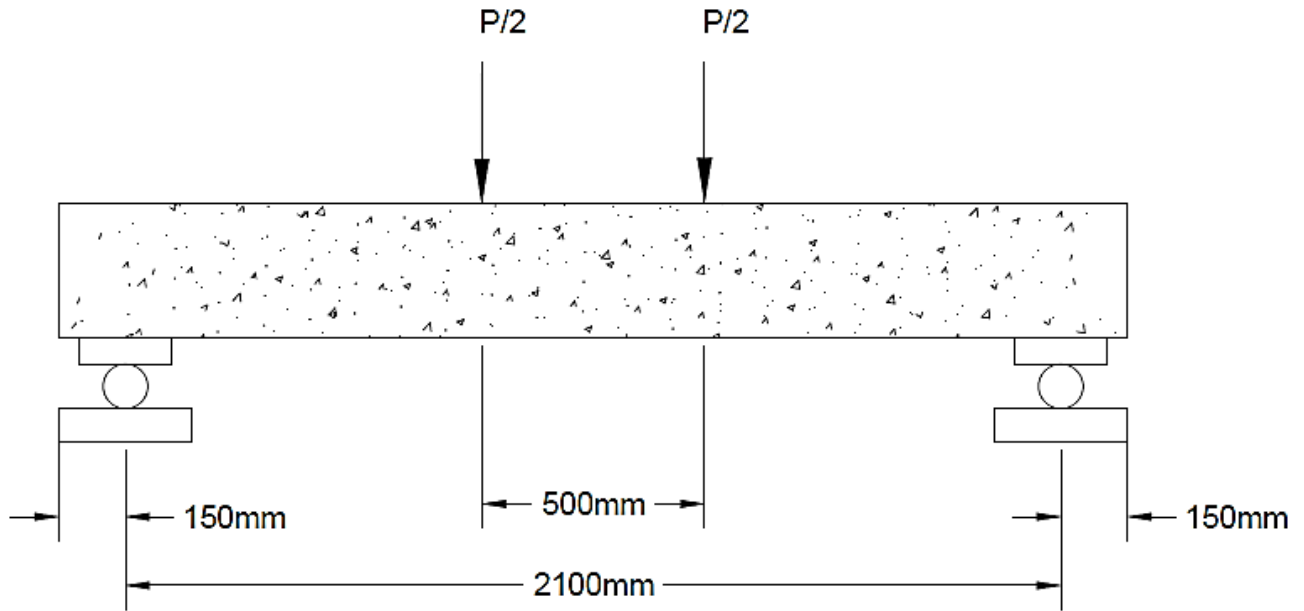


Figure 4: Test details

^^



Figure 5: Actual test set up

### 3.3. Materials specifications

The concrete type used in these finite elements is Ordinary Portland cement-based concrete (OPCC). The mechanical characteristic of this concrete is shown in the [Table 2](#) below.

Table 2 Concrete properties for ANSYS Finite Element Modeling

Type of Concrete	OPC	Unit
28-day Compressive strength	41.0	Mpa
Modulus of Rupture	4.05	Mpa
Elastic Modulus	30000	Mpa
Poison's ratio	0.2	-
Density	2300	(Kg/m <sup>3</sup> )
Uniaxial Tensile Strength	3.107	Mpa
Biaxial Tensile Strength	51.75	Mpa
Uniaxial Compressive Strength	45	Mpa

..

Two GFRP bars have been used, each of 16 mm diameter as the main reinforcement in tensile, while in the compression region, two rods with a diameter of 10 mm have been utilized. Also, the diameter of pre-bent stirrups reinforcement is 10 mm spaced at 70 mm within the two shear spans only. Table 3 demonstrates the mechanical properties of these rebars, while Figure 6 presents its stress-strain response.

Table 3 GFRP mechanical properties and characteristics

Reinforcement	Unit	Moment bars	Shear stirrups	Compression bars
Net Diameter	(mm)	15.2	9.2	9.2
Area	(mm <sup>2</sup> )	181.5	66.5	66.5
Density	Kg/m <sup>3</sup>	2100	2100	2100
Young Modulus	GPa	60	60	60
Poisson's Ratio	N.A.	0.25	0.25	0.25
Tensile Ultimate strength	MPa	978	978	978
Ultimate strain	N.A.	0.0171	0.0171	0.0171
Compressive Ultimate Strength	MPa	400	400	400

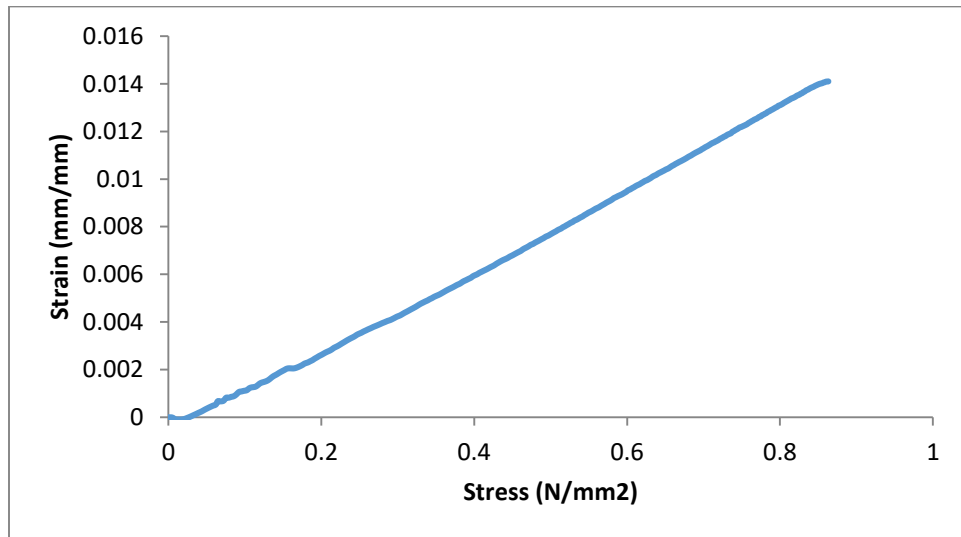


Figure 6 GFRP rebar stress-strain relationship

..

### 3.4.Types of Elements

#### Concrete

#### SOLID185

**SOLID185** is a feature that is used to model three-dimensional solids structural elements. It comprises eight nodes, each with three degrees of freedom: translations in the nodal x, y, and z directions. The element (SOLID185) is capable of plasticity, hyperelasticity, stress stiffening, creep, large deflection, and significant strain. It also can simulate deformations of almost incompressible elastoplastic materials and completely incompressible hyperplastic substance using mixed formulations. [Figure 7](#) below illustrates the geometry of SOLID185 element

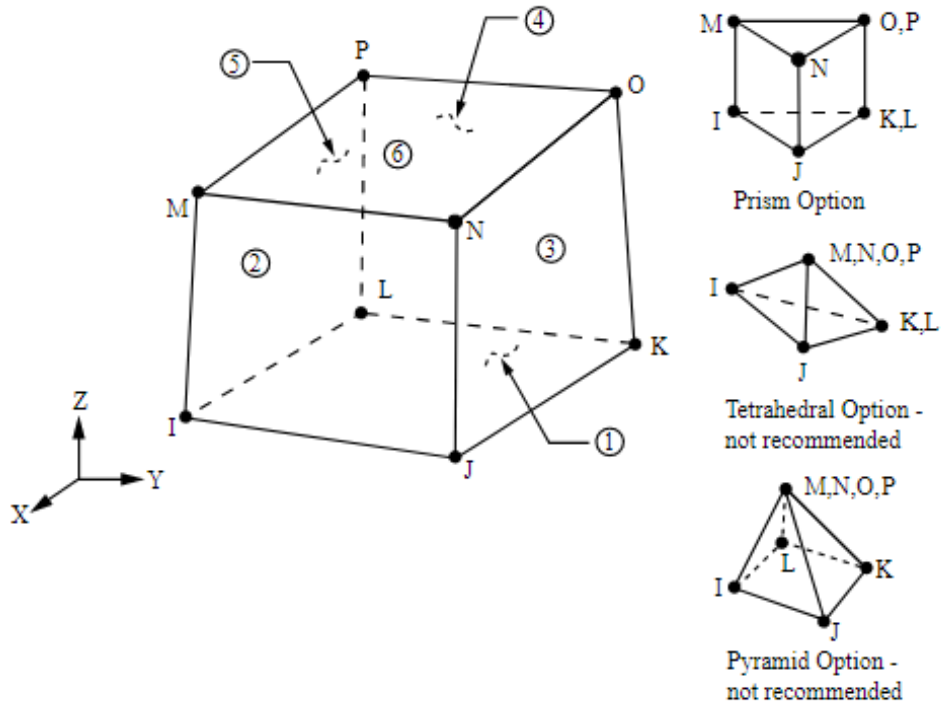


Figure 7: Geometry of the SOLID185element

^^

## GFRP bars

### REINF264

The REINF264 can reinforce several elements such as 3-D link, beam, shell, and solid elements. The element can be used to simulate any orientation of reinforcing fibres. Each fibre is represented as a separate spar with only uniaxial stiffness. REINF264 can plasticity, stress stiffening, creep, large deflection, and significant strain. [Figure 8](#) [Figure 9-\(2,3\)](#) below shows the geometry of the REINF264 element and the Coordinate System

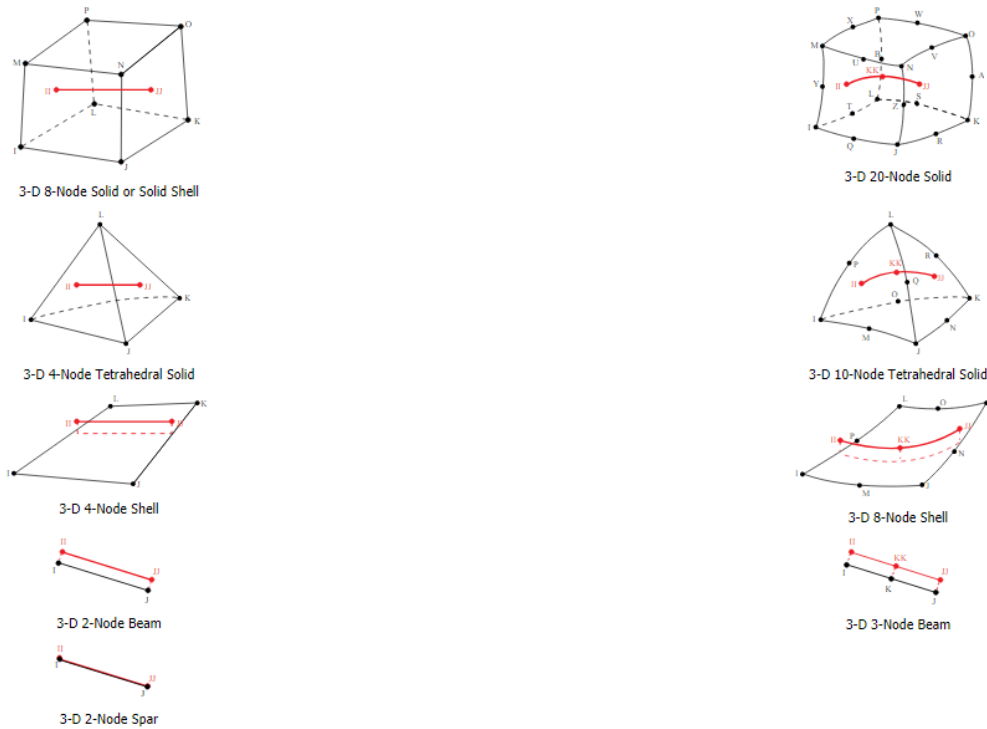


Figure 8: Geometry of the REINF264 element

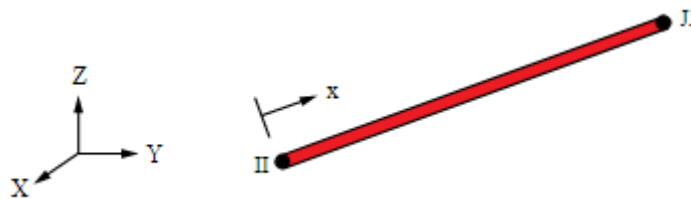


Figure 9: Coordinate System of the REINF264 element

..

The [Table 4](#) below demonstrate the Elements expression:

Table 4: The expression of the Elements

<b>No. Of Element</b>	<b>Type of Element</b>	<b>Express</b>
1	SOLID185	Concrete
2	REINF264	longitudinal of GFRP bars
3	REINF264	GFRP Stirrups

### 3.5. Meshing:

The elements that comprised the finite element model had to be appropriately selected to provide a credible simulation of the real conduct action of the concrete beam reinforced with GFRP. The mesh size was deliberately chosen to achieve high precision with a short computing time. The ANSYS 2021 software was used for the study. The number of steps that have been selected was 25 steps with five sub-steps for GFRP rebar. The load at the last stage in the FE model was -360000KN.

..

## Instrumentation

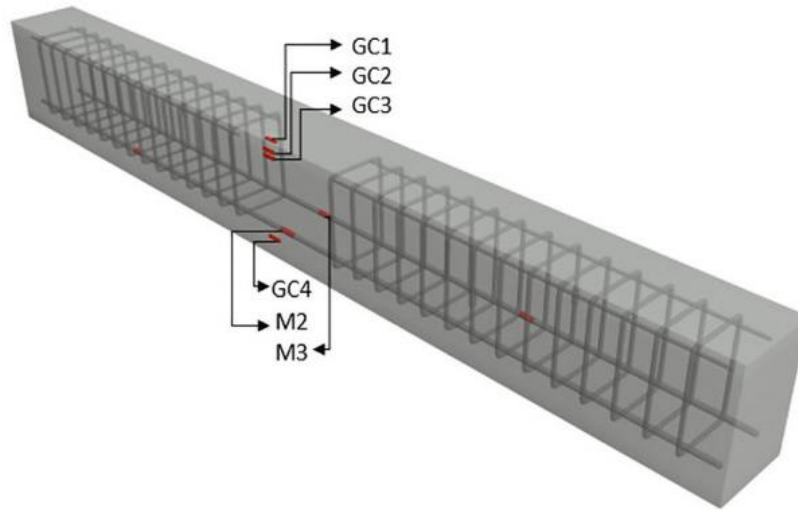


Figure 10: strain-gages spots

Figure 10 demonstrates the locations of the gages on the specimens. As appears in the figure, two strain gages (M2, M3) were placed inside the beam at the middle of the main reinforcement of GFRP rebars. The GC1 gauge was plotted at the topmost surface of the middle beam. Also, the other two gages (GC2, GC3) were placed in the depth of 20 mm and 35 mm, respectively, from the upper surface of the beam (GC1). The spots of strain gages were used in the experiment to compare the results with FE analysis.

“

## Chapter 4: Results

## 4. Chapter 4: Results

### 4.1. Non-Linear results

The cumulative applied load to the EE model in the nonlinear analysis is divided into a set of load increases known as load steps. The stiffness is determined at the end of each incremental outcome. The model's matrix is modified to account for nonlinear shifts in structural stiffness before moving on to the following step. Using Newton-Raphson equilibrium iterations, the ANSYS software renews the model stiffness. At the end of each step, the iterations of the Newton-Raphson equilibrium have convergence. Within acceptable ranges, [Figure 11](#) below depicts the use of the Newton-Raphson method in lone freedom degree.

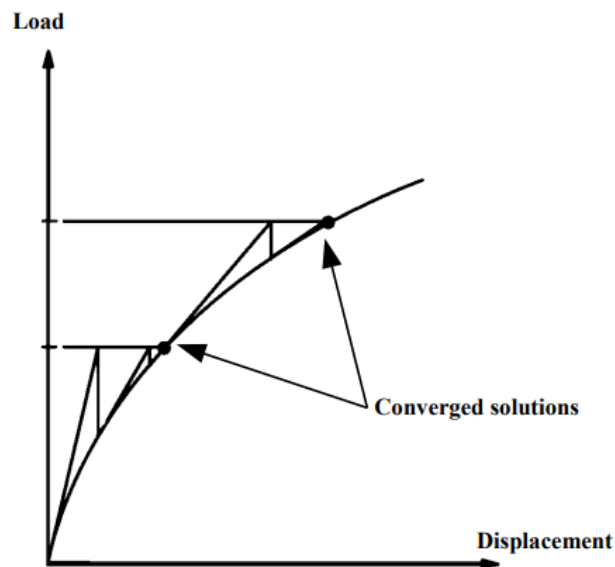


Figure 11 Iterative Newton-Raphson result (2 load increments) (ANSYS)

..

Convergence conditions for rigid reinforced concrete components depend on load and deflection in this analysis and the convergence allowance boundary initially chosen by ANSYS software.

## 4.2. Load Deflection

ANSYS software was used to create a FE method (FEM) to mimic the beam response under incremental displacement. The deflection of the mid-span was recorded and discussed at different loading stages. Those are pre-initial cracking, post-cracking, and failure. All these positions were graphically compared.

Figure 12 and Figure 13 compare the deflection response to load acquired from the FEM and the ACI 440.1 Code [57], as well as with the experimental findings for the beam [70-72, 90, 92]. The y-axis presents the Load in "KN," and the x-axis shows the mid-span deflection in millimetres.

Looking at the first section in Figure 12 of the load and deflection patterns, the initial response of the FEM is a little stiff than the experimental outcome in the linear domain. The load at cracking of the "SOLID 185" based FE model is 28.0 KN, identical to the experimental result's load of 28.0 KN. This indicates the accuracy of the results of the FE model. After the initial cracking, the trend of the outcome of the FEM matches with the experimental findings. Finally, the model's final load of 171.9 KN is just 0.1% less stiff than the experimental data's ultimate load of 171.8 KN. However, the deflection at maximum load is inaccurate because the model cannot detect the cracking before the

..

concrete crushing failure at the compression zone, resulting in lower stiffness and lower failure deflection.

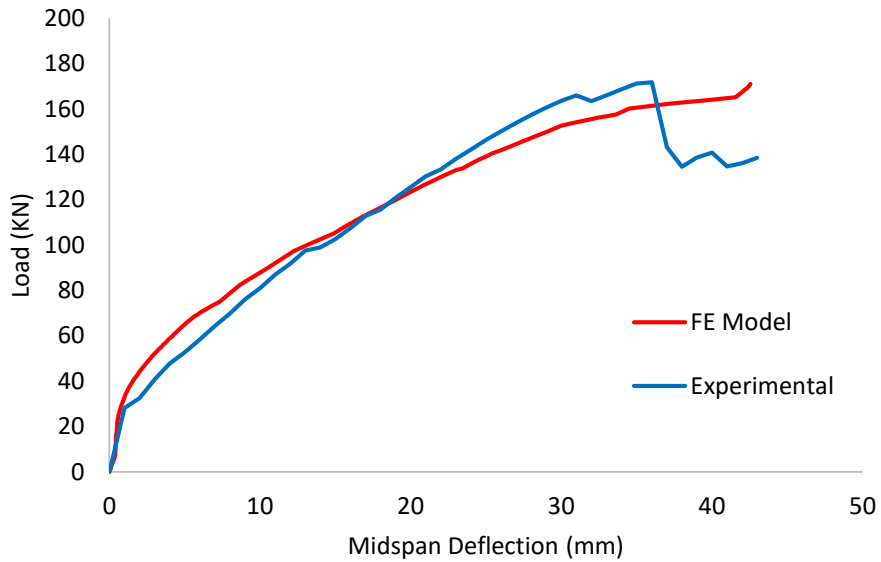


Figure 12: Slopes of load-deflection for the FE and experimental findings

The incremental theoretical correlation is obtained for each experimental load step by utilizing the ACI mentioned above formula and compared with the Finite Element model and the experimental findings and presented in [Figure 13](#) and [Figure 14](#).

[Figure 13](#) illustrates the Load deflection plots for the outcomes obtained from the FE model (SOLID185) and the ACI 440.1. The initial section demonstrates that the stiffness of the ACI model is marginally higher than the FE model. The initial crack of the ACI 440.1 code was 28.1 KN, while the initial crack of the "SOLID 185" based FE model is 28.0 KN which is around 0.3% stiffer than the FE model. The variance in the stiffness

..

after the initial cracking segment was almost the same. At the ultimate load, the ACI 440.1 code was 0.4% higher than FE model SOLID185.

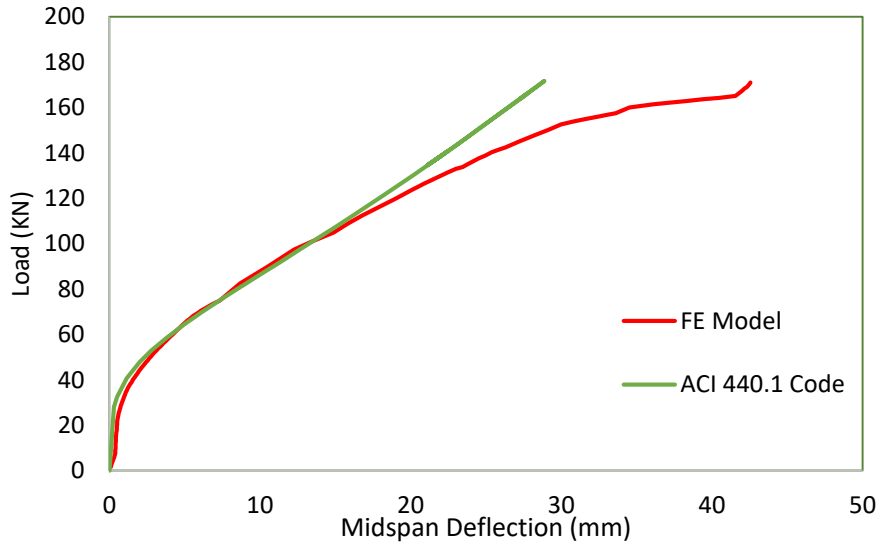


Figure 13: Slopes of load-deflection for the FE and ACI 440.1 models

Finally, [Figure 14](#) below concludes that, in general, the load-deflection plots from the FE analyses for beam match the experimental outcome and the ACI 440.1 guideline quite well. In the linear spectrum, the ACI 440.1 code load-deflection plots are stiffer than the finite element plots, while the experimental outcomes plots were the lowest in stiffness. The finite element analysis findings for the beam (SOLID 185), the experimental data of the samples, and the ACI 440.1 code variants from 28.0 kN to 28.1 kN for the first cracking load. The difference in the percentage of stiffness for each of the data shown in [Figure 14](#) ranges from 0 to 0.3 percent, which is considered highly accurate. After the first cracking, the stiffness of the ACI model is greater than the experimental results of the specimens and the FE model. At that region, the deflection values from the ACI model are lower than the others. Hence, the ACI under-predicts the actual deflection response at the post-cracking

..

stage, while the deflection of the FE model outcome is similar to the experimental value. However, the stage before the concrete crushing is challenging to predict due to the uncertainties of the behaviour with the progression of the cracks before in the compression zone.

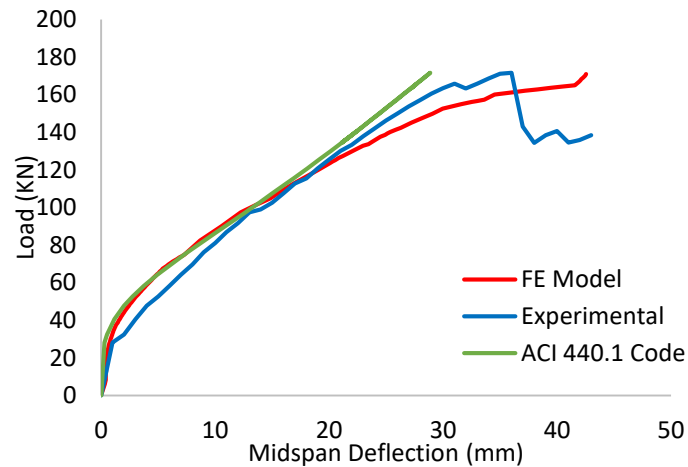


Figure 14: Load-Deflection Plots of FE model, experimental samples, and ACI code

The higher stiffness in finite element models may be due to several reasons. Micro-cracks in the concrete are present to some extent due to drying shrinkage and treatment. Also, the finite element models do not account for the micro-cracks; this will lead to incremental stiffness of the beams. The finite element analyses presume an excellent relationship amid the concrete and GFRP rebars, but this is not the case with the experimental outcome. The composite interaction between the concrete and GFRP rebars is missed as the bond slips. As a result, owing to conditions that are not considered within the FEM, the average stiffness of the actual experimental results can be lesser than

..

predicted. As a result of variables not accounted for in the simulations, the average stiffness of the individual beams can be lower than expected by the FEM.

All the load-deflection diagrams can be allocated into three distinct divisions. The first section is the initial linear region, which is the part that extends until cracking occurred in the beam and is also called the pre-cracking region. There is an apparent change in slope when the crack is initiated; this shows the three models appropriately account for the initial un-cracked load-deflection behaviour. The ACI 440.1 model proposes conservative values, while the FE model predicts this section more accurately than the experimental behaviour. However, the FE model does not establish the transition between the pre-and the post-initial crack behaviour. The FE model does not account for the micro-cracking and the intercourse between the concrete particles that cause the sudden stiffness changes.

The second segment is the post-initial cracking phase; this phase is observed to be non-linear. In this region, the stiffness is reduced owing to the cracking of concrete in the tension section. The Solid185 based model was successfully able to simulate the post-initial cracking with acceptable accuracy. The experimental lines and the analytical lines meet together and increase gradually. Also, it is possible to notice the convergence of the lines from each other, which indicates the correctness, mastery, and simulation of the work very close to reality.

..

The third stage is the stage that shows the ability of the beam to withstand the applied load after the occurrence of concrete crushing. The FE model cannot capture the post-failure behaviour because of the current limitation of ANSYS software and the Soild185 integration. However, the ultimate load, where surprisingly the concrete crushing took place.

Figure 15 and Figure 16 below show the loading and unloading beam deflection of experimental samples.



Figure 15: the beam under applied load



Figure 16: the beam after applied load

..

## Carrying capacity

### 4.3.Loads at First Cracking

The load at that the crack initiated " $P_{cr}$ " could be noticed from the load-deflection model of the FE model by identifying the loading step at which the curve shows a transition in stiffness (initial section) where the finite element analysis's first cracking load is the load step which is the first sign, indicating the occurrence of a crack in the concrete, appears in the model. The experimental samples'  $P_{cr}$  was observed during the test, while the theoretical  $P_{cr}$  value was obtained from eq (cracking moment). Table 5 compares the first cracking loads of the FE model, the experimental samples, and the ACI 440.1 code and the accuracy compared to the experimental.

Table 5: Accuracy and Comparison of Theoretical model (ACI), Experimental Work and ANSYS at initial cracking load

Type of test	Units	The percentage different
Experimental	28.0 KN	-
ANSYS	28.0 KN	0.0%
ACI	28.1 KN	0.35%

The percentage of the variance among the FE analysis with experimental samples and ACI 440.1 results does not exceed 1%, which appears the accuracy of the FE analysis. The highest stiffness at initial cracking occurred through the theoretical model (ACI 440.1) 28.1 KN, while the FE model and experimental findings were identical. It can be observed from Table 5 the excellent accuracy of the results obtained from the ACI 440.1 code.

..

#### 4.4. At failure loads

Table 6 compares the FE simulations, experimental outcome, and ACI 440.1 model. ANSYS model estimates the ultimate strength of the beam by 0.06%-0.12%, which is an excellent approach.

Table 6: Accuracy and Comparison of Theoretical model (ACI), Experimental Work and ANSYS at failure load

Type of test	Units	The percentage different
Experimental	171.8 KN	-
ANSYS	171.9 KN	0.061%
ACI	171.7 KN	0.058%

#### 4.5. Tensile Strain of FRP

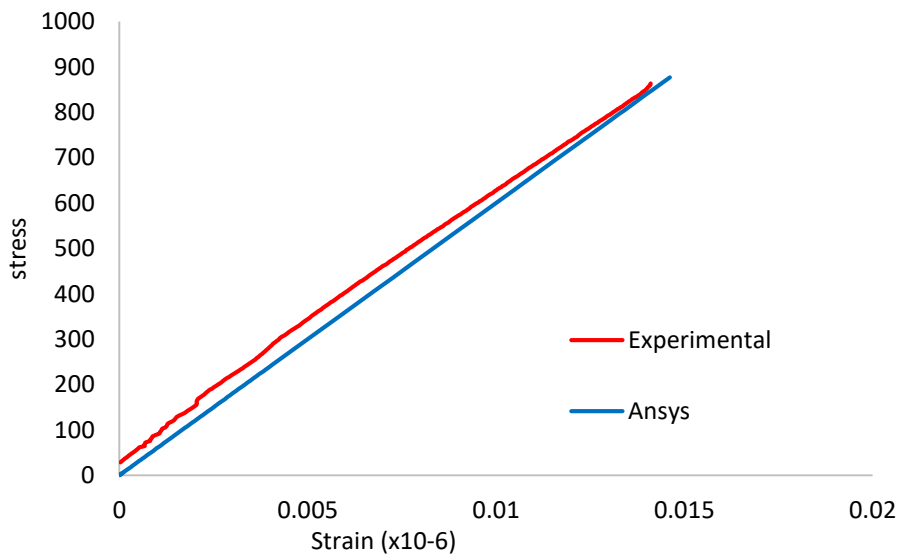


Figure 17: Tensile stress-strain curve of GFRP rebar for experimental and FE model

^^

Figure 17 illustrates the comparison of the tensile stress-strain plots for the experimental and FE model. Note that the Y-axis is the beam's stress, while the X-axis represents how much the beam was a strain. It can be observed from the figure above the extent of the correlation of the results obtained from the FE analyses with experimental findings, which gives an excellent agreement for the precision of FE modelling. Although the products are closely related, the experimental results are slightly higher than the FE model.

Figure 18 and Figure 19 below illustrates the stress and the strain of the FE model taken from ANSYS 2021 software.

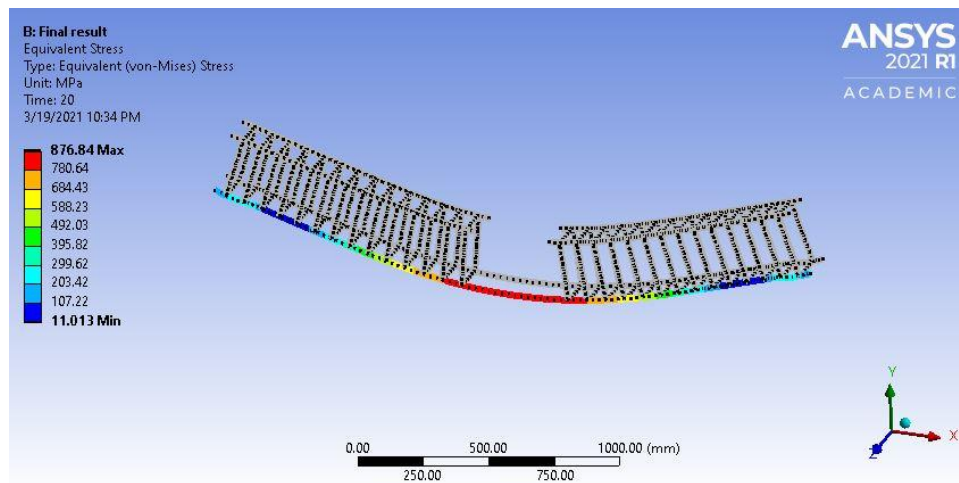


Figure 18: The stress of GFRP rebar (ANSYS 2021)

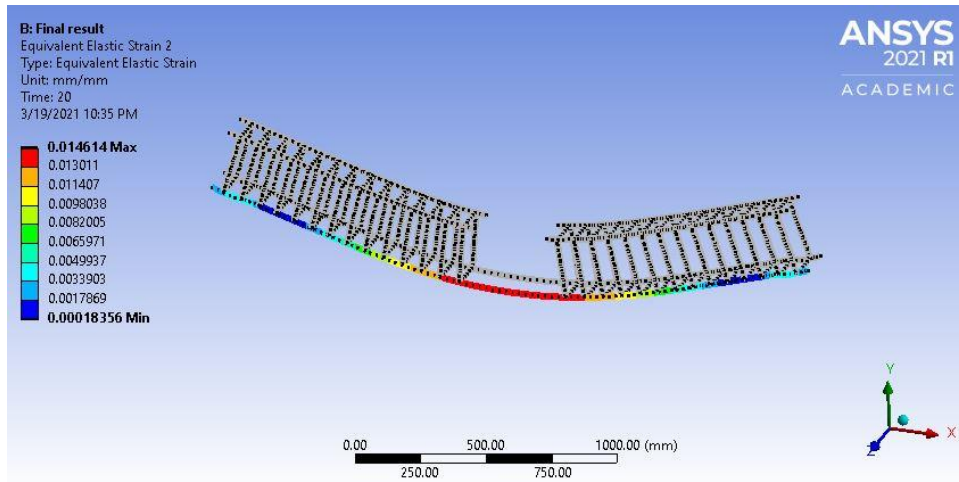


Figure 19: The strain of GFRP rebar (ANSYS 2021)

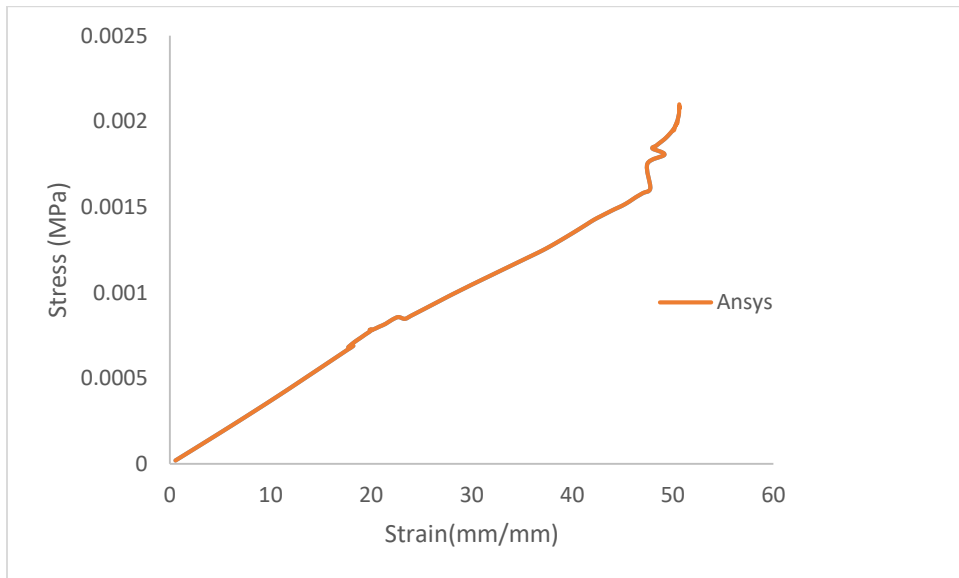


Figure 20: Compressive stress-strain curve of concrete of FE model

Figure 20 demonstrates the results of stress-strain plots of concrete obtained from the FE model using ANSYS software. The concrete stress is heading in a linear behaviour up to when the failure occurs. The compressive uniaxial stress-strain response for the concrete design was gained in this analysis by using a multilinear isotropic stress-strain relationship.

^^

Figure 21 and Figure 22 shows the stress-strain of the concrete given from Finite Element ANSYS 2021 software.

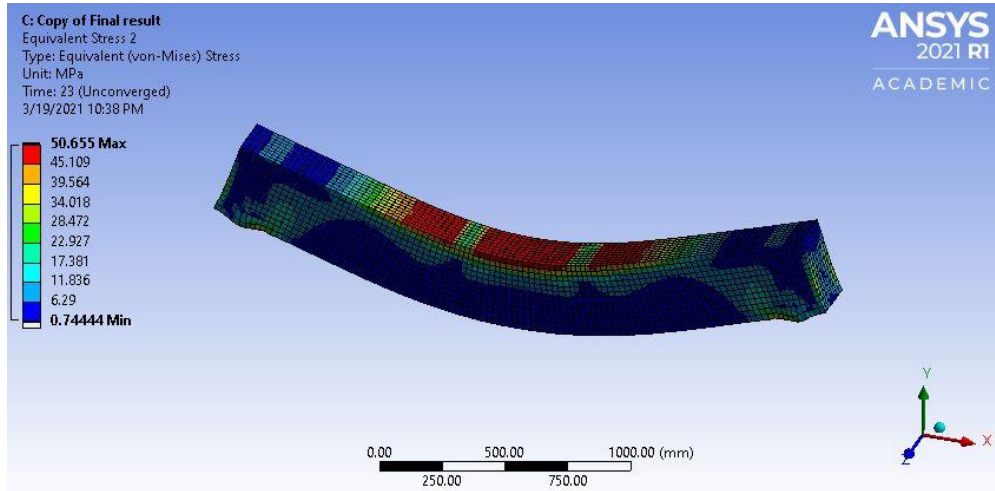


Figure 21: The stress of Concrete (ANSYS 2021)

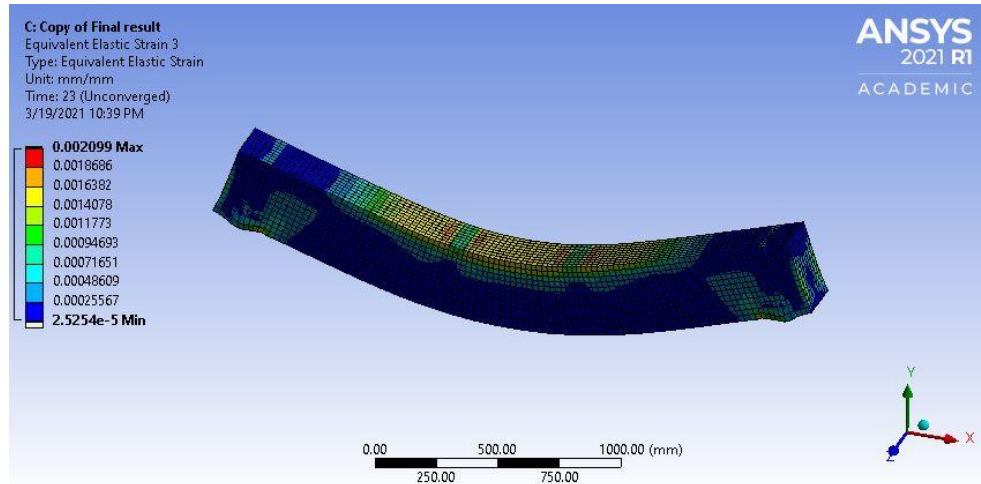


Figure 22: The strain of Concrete (ANSYS 2021)

..

## 4.6. Experimental findings

### 4.6.1. Types of failure

The concrete crushing in the compression region caused all of the beams to fail. The strain gages fitted in the center of the two flexural GFRP rebar produced results that did not surpass the manufacturer-certified rupture strain ( $f_u^*=0.0171$ ). This demonstrates how concrete crushing mode is the primary failure mode for entirely evaluated beams. According to ACI 440 guidelines, this is the predicted failure because it is more ductile and less destructive than GFRP rupture. This is much more sudden. [Figure 23](#) illustrates the OPCC beam at failure mode.



Figure 23: Beam at failure mode

According to [Figure 23](#), numerous tensile cracks are evident, and the concrete has been crushed in the compression region due to the applied loads. The bending of the beam owing to loading is visible in the illustration. The diagram also depicts the curvature of the beam as a function of loading.

..

#### 4.6.2. Cracking patterns

Figure 24 and Figure 25 depict the cracking patterns of the checked beams. The friction side of the constant moment region developed tiny cracks in many of the examined beams. As the load raised, additional flexural cracks developed, first in the constant moment region, then in the shear span. Cracks further aside from the middle of the member originated with a more significant load than cracks closer to the center of the beam. Cracks that occurred under higher loads showed a steep slope away from the vertical axis. The inclination of the cracks grew as they spread higher, and they moved nearer to the increased load. This is due to the beam's high bending due to the added load, which is normal behaviour.

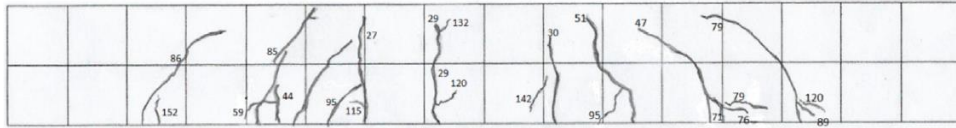


Figure 24: Cracking patterns of OPCC beam



Figure 25: Cracking patterns of Actual OPCC beam

..

#### 4.6.3. Strain development

Figure 26 displays the strain results on the GFRP bar with the implemented load at four places, two on either side of the bisection shear span (M1, M4) and two on each center span bar (M2, M3). As predicted, strain results in the middle span of the pure constant moment region (1.05 from any side) are more significant than strain values in the shear region at the mid of the member (0.4m from either support). If a stress region break happens at the strain gauge spot, the strain on the GFRP rebar develops. At the beginning of the graph, the steep slope, similar to load-deflection patterns, reflects the beams' un-cracked state. In the tension zone, the concrete also aids in tensile stress resistance. Once cracking, the concrete can no longer withstand tensile stresses, and the GFRP rebar tends to strain, as shown by the variation in inclination caused by the cracking load.

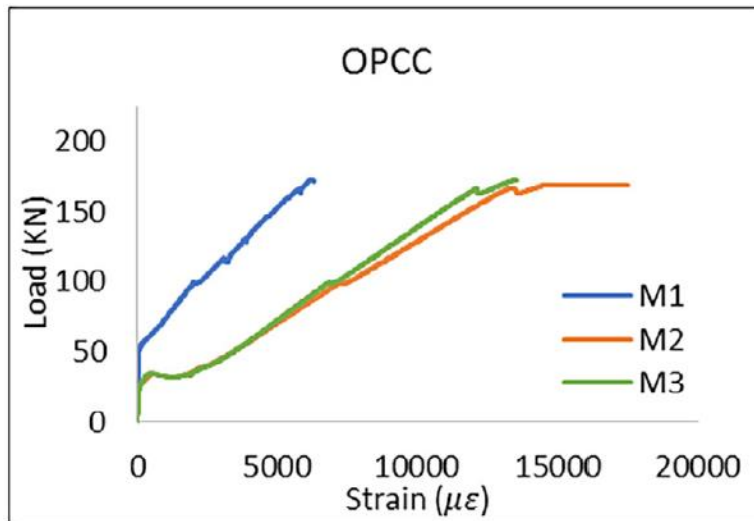


Figure 26: The flexural of GFRP rebar Load-Strain curve

..

That is also demonstrated in [Figure 27](#), in which the strain formed on the face of concrete at the particular time as the GFRP reinforcement overlaps the strain created in the GFRP reinforcing rebar. The concrete strain gauge began collecting results after the cracking load was achieved, and the GFRP rebar strain rate grew dramatically. The rebars were strained steadily up to the strain gauge was fully strained.

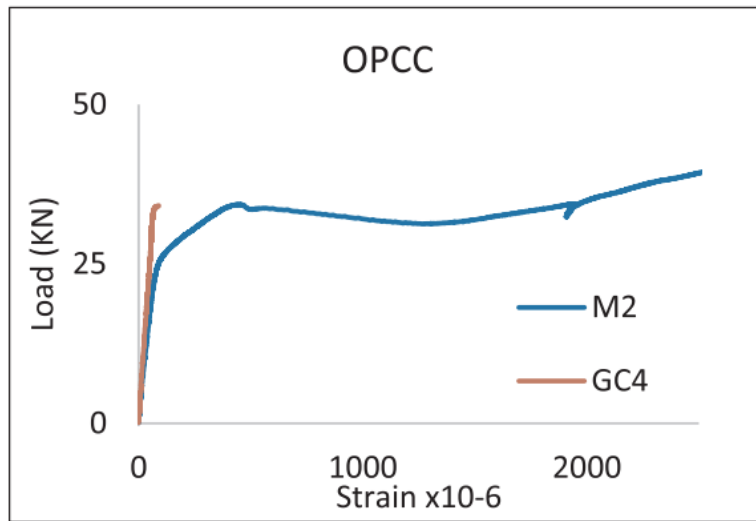


Figure 27: the load-strain curve of un-cracked condition beam

According to ACI 440 guidelines, the strain at the mid-span of the GFRP rebars did not rupture, and the member was not over-reinforced since the GFRPs remained linear with the load. The strain values measured by M1 and M4 at the half shear period had been lesser during similar load values, showing a wide stress distribution along the flexural bars. Thus, adequate bond characteristics among the matrix and the reinforcing.

..

To evaluate the strain, four strain gages installed to the outer surface of the member corresponding with the depth of the mid-span-section at depths of 0.0 (GC1), 20 mm (GC2), 35 mm (GC3), and 250 mm (GC4) from the upper surface. Obtain the strain distribution along the beam at various load levels profundity. The strain amounts from these strain gauges at multiple loadings were utilized to create the loading section's strain profile, as is shown in [Figure 28](#). The concrete reaches its ultimate strain in over-reinforced members, and the breakdown is controlled by concrete crushing.

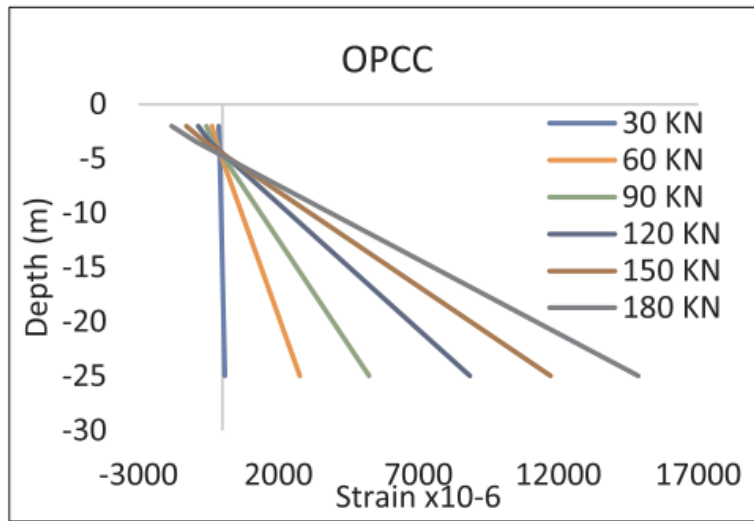


Figure 28. Profile of strain across the midsection's depth.

“

## Chapter 5: Discussion of Results

..

## 5. Chapter 5: Discussion of Results

Pearson Product Moment Correlation (PPMC): It depicts the correlation among two groups of results. It can be calculated by using the Microsoft Excel program, as shown in [appendix B](#).

The equations return a value ranging from -1 to 1, where:

- A score of **1** demonstrates a perfect positive relationship.
- A score of **-1** demonstrates a strong negative relationship.
- A consequence of **zero** means that there is no relationship at all.

As shown in [Figure 29](#) below, the correlation trend between the Deflection in (mm) and Load in (KN)

For experimental data, it indicates a very high positive correlation relationship.

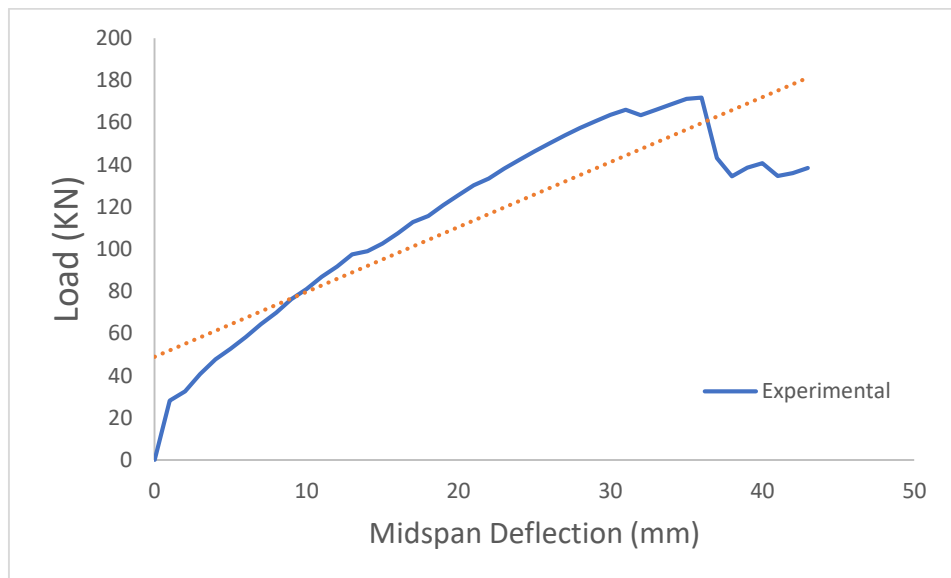


Figure 29: Linear trend line of experimental correlation

..

Figure 30 demonstrates a very high positive correlation relationship between the Deflection in (mm) and Load in (KN) of ANSYS results.

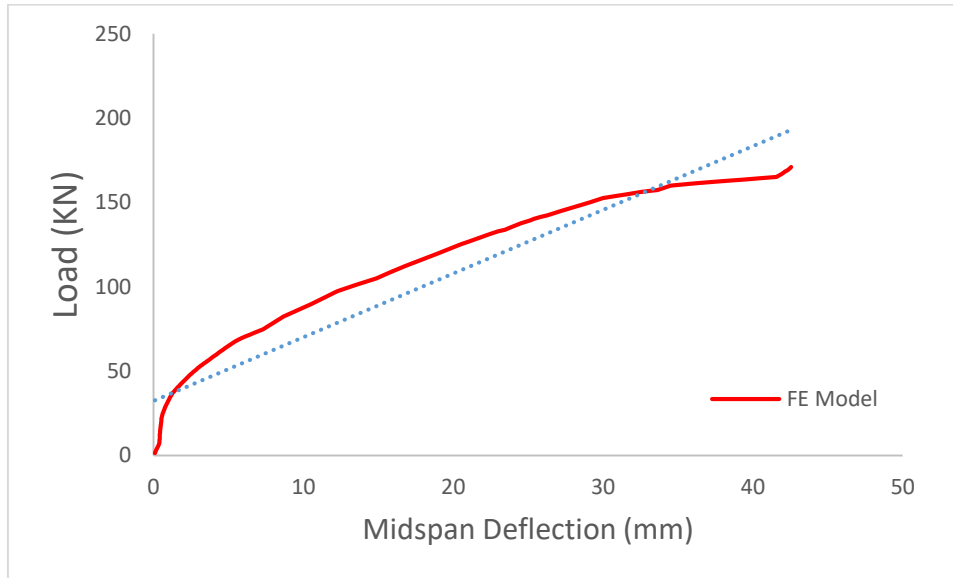


Figure 30: Linear trend line of FE Model correlation

Figure 31 illustrates a very high positive correlation relationship of the Deflection in (mm) with Load in (KN) for ACI calculations.

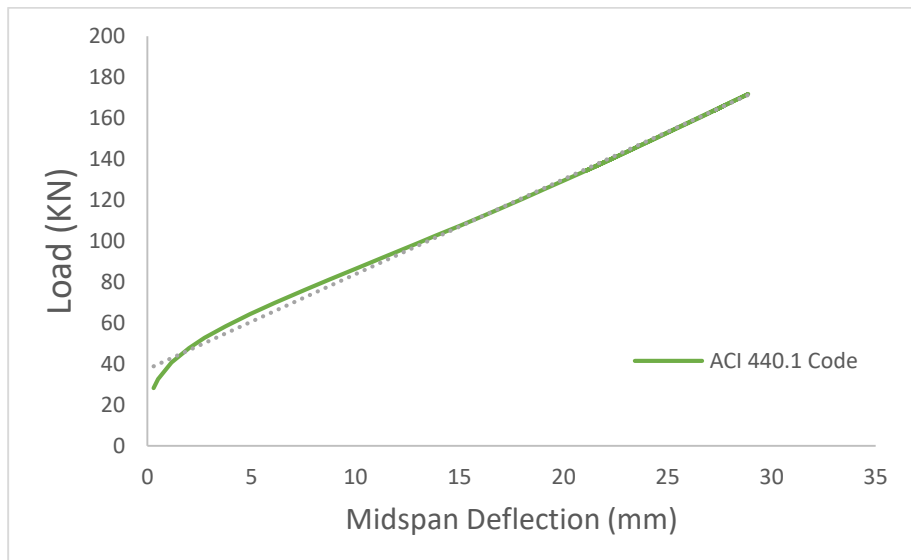


Figure 31: Linear trend line of ACI 440.1 Code Model correlation

..

The [Table 7](#) below demonstrates the value of the (r) Coefficient of three different models.

Table 7: The “R” coefficient of the three models

<b>Model type</b>	<b>Correlation Value (R)</b>
Finite Element Analysis	0.95
ACI	0.99
Experimental	0.97

In conclusion, all the figures above give a positive correlation between the two variables: any rise in a single variable, a specific proportional height in the other. [Figure 32](#) shows the correlation factor between the Strain-Stress variable.

^^

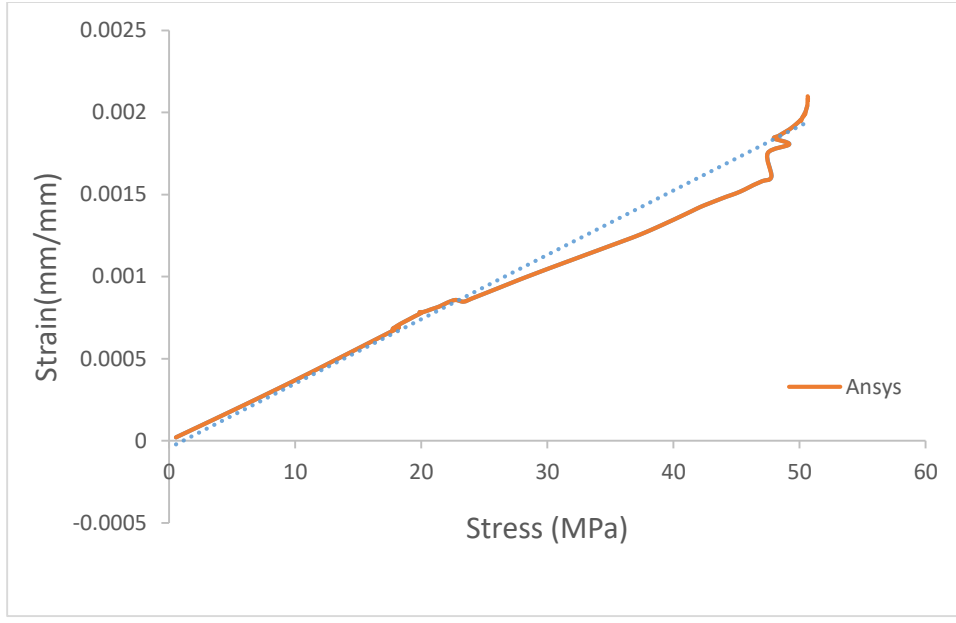


Figure 32: Linear trend line of Strain-Stress correlation of Concrete by FE Model

The correlation factor “R” of Figure 32 is **0.99**, indicating a very high positive relationship between strain and stress variable.

..

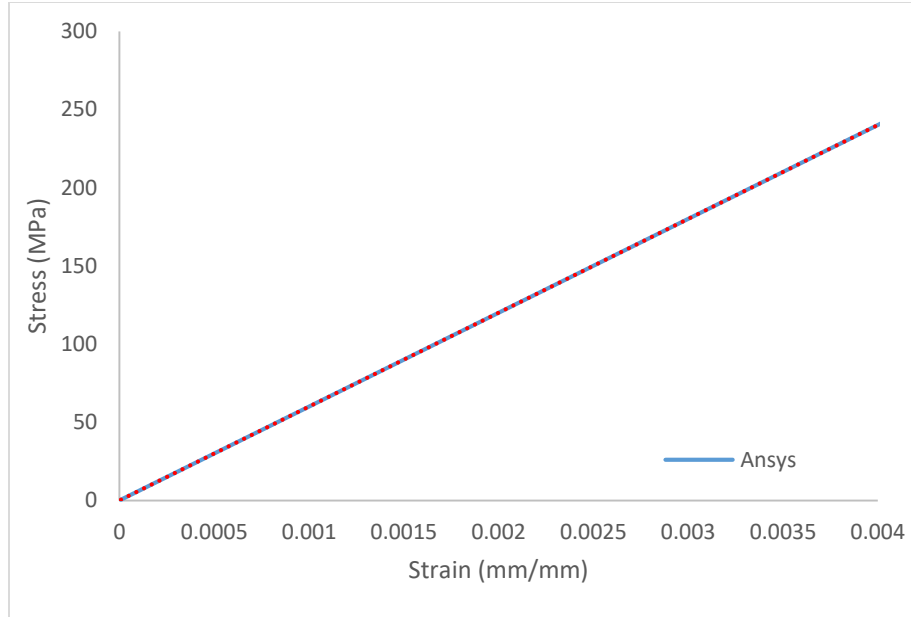


Figure 33:: Linear trend line of Stress-Strain correlation of GFRP rebar gained from FE Model

The correlation factor (R) of Figure 33 is **-0.11**, indicating a very low negative relationship between strain and stress variable of GFRP rebar in the FE model.

ANOVA test is a method for determining whether test or analysis findings are significant. In other words, it assists you in deciding whether you can refuse the null hypothesis or consider the alternative hypothesis.

..

One-way ANOVA test means there is only one independent variable in a one-way method (with two levels). It is also can make a comparison between the means of many groups. It is possible to compute it using the Microsoft Excel software, as seen in the process in [Appendix C](#).

For one-way ANOVA, the below are the typical hypotheses:

- Null: The means of all these groups are the equivalent
- Alternative: Not all means of a group are created equivalent

The most critical value in the ANOVA test is the p-value. It states whether admit or discard the null hypotheses. Reject the null hypothesis if the p-value is below the significance range (typically 0.05). In the data shown in the [Table 8](#) below, the p-value was 0.83, which is greater than  $\alpha$  0.05, indicating the null hypothesis is accepted.

Table 8: Outcomes of the ANOVA single factor assessment

ANOVA: Single  
Factor

SUMMARY						
Groups	Count	Sum	Average	Variance		
Load (KN) Experiment	43	4990.47	116.06	2165.44		
ANSYS	43	5108.87	118.81	1747.75		
ACI	31	3385.27	109.20	1810.80		

ANOVA						
Source of Variation	SS	df	MS	F	P-value	F crit
Between Groups	1707.12	3	569.04	0.29	0.83	2.68
Within Groups	218677.62	113	1935.20			
Total	220384.74	116				

..

The other criteria that can be used accept or reject the null hypotheses by looking for F critical and F calculated. If F calculated exceeds F crit, the null hypothesis is denied. In the outcome of results, as shown in the [Table 8](#) above, the F crit was bigger than F calculated that is means the null hypothesis is accepted. The [Figure 34](#) below illustrates the rejected region in red color, which is the region greater than 2.68

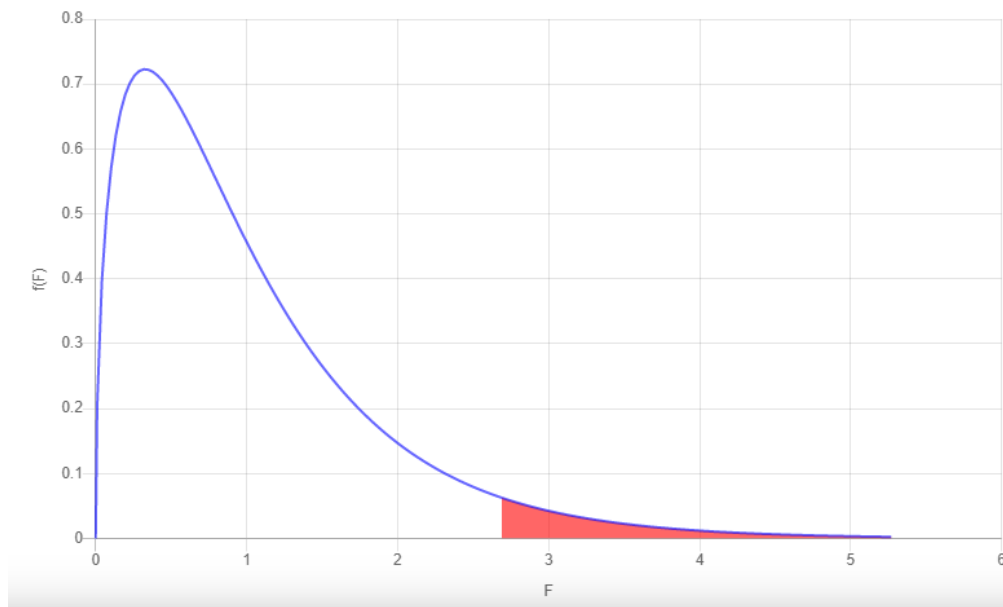


Figure 34: Critical Value of F-distribution 2.68

The outcomes of the ANOVA test generate the sum of squares among groups and the sum of squares within each group.

The ANSYS program results are compatible with the experimental results within 10% error rate regarding research outcomes and literature review. The type of failure was a concrete crushing failure at ultimate load, which is reliable with the previous results [\[83\]](#).

..

The findings observed are considered models that are effective in terms of time and cost. The ANSYS system is a feasible and functional system with consistent results, as verified according to the research prepared by [88].

The ANSYS design model demonstrated the ability to effectively simulate the mechanical characteristics of concrete and steel reinforcement GFRP structures. This was also observed in another study by [87].

The study demonstrated the differences and comparisons between three different models using three methods: simulation using the ANSYS software, US code ACI 440.1, and experimental work. The research findings utilizing three strategies are both functional and valid. This was verified using diagrams and error ratio calculations and statistical models and equations such as the Pearson Product Moment Correlation (PPMC) test and one-way ANOVA test.

“

# Chapter 6: Summary and Conclusion

## 6. Chapter 6: Summary and Conclusion

This study examined the flexural behavior of GFRP reinforced concrete beams utilizing a nonlinear finite element analysis. The research considered the beams' pre-initial cracking, post-cracking, failure, load mid-span deflection, and stress-strain. Both material and geometric nonlinearities were taken into account in the finite element model.

- ANSYS21 FEA models are now able to simulate reinforced concrete beams with GFRP rebar.
- The FEA findings are pretty similar to the results obtained from the experiments.
- Given failure load estimating, the variance between FEA model findings, experimental results, and ACI 440.1 theoretical models within a 10% margin of error.
- All GFRP-reinforced beams failed at ultimate load owing to concrete crushing in the compression region.
- According to ACI requirements, all of the beams failed to owe to concrete crushing when they had been created to be over-reinforced.
- The initial cracking load applied to the reinforced concrete beam suits ACI equations very well.
- For all beams, the load-deflection curve behaves linearly in the first phase, reflecting the beam in its un-cracked state, followed by a nonlinear response with a reduced slope, representing the beam after cracking up to the maximum load.
- The load-strain relationship of GFRPs behaved linearly after  $\epsilon_{cu}$  Moreover, up to concrete crushing, this shows that the GFRP rebar did not

^^

rupture and that the beams were over-reinforced, indicating that the manufacturer's final rupture strain was underestimated.

## 7. References

- [1] Y. H. Huang and Y. C. Guo, "Review of durability of Fiber Reinforced Polymer (FRP) reinforced concrete structure," in *Applied Mechanics and Materials*, 2014, pp. 1651-1654.
- [2] P. Böer, L. Holliday, and T. H.-K. Kang, "Independent environmental effects on durability of fiber-reinforced polymer wraps in civil applications: a review," *Construction and Building Materials*, vol. 48, pp. 360-370, 2013.
- [3] P. Huang, H. Zhou, X. Zheng, and X. Guo, "On the experimental method for durability measurement of RC members strengthened with FRP served in hot and humid environments," *Journal of Experimental Mechanics*, vol. 26, pp. 603-610, 2011.
- [4] N. F. Grace and S. Singh, "Durability evaluation of carbon fiber-reinforced polymer strengthened concrete beams: experimental study and design," *ACI Structural Journal*, vol. 102, pp. 40-53, 2005.
- [5] Y. Y. Y. M. Z. Yan and L. Jie, "Experimental study on durability of basaltic fiber reinforced polymer [J]," *Industrial Construction*, vol. 6, 2007.
- [6] L. C. G. D. Z. Jun, "Experimental study on durability of FRP entirely-wrapped concrete cylinders and FRP strip-wrapped concrete cylinders under wet-dry cycles in salt solution [J]," *China Civil Engineering Journal*, vol. 11, 2009.
- [7] A. A. Mufti, N. Banthia, B. Benmokrane, M. Boulfiza, and J. P. Newhook, "Durability of GFRP composite rods," *Concrete international*, vol. 29, pp. 37-42, 2007.
- [8] S. Li, H. Ren, C.-k. Huang, and M.-h. SHI, "Combined effects of temperature and alkaline solution on durability of FRP sheets," *Journal of Building Materials*, vol. 1, pp. 94-99, 2010.
- [9] J. W. Chin, K. Aouadi, M. R. Haight, W. L. Hughes, and T. Nguyen, "Effects of water, salt solution and simulated concrete pore solution on the properties of composite matrix resins used in civil engineering applications," *Polymer composites*, vol. 22, pp. 282-297, 2001.
- [10] F. E. Tannous and H. Saadatmanesh, "Durability of AR glass fiber reinforced plastic bars," *Journal of Composites for Construction*, vol. 3, pp. 12-19, 1999.
- [11] V. Karbhari and S. Zhang, "E-glass/vinylester composites in aqueous environments—I: experimental results," *Applied Composite Materials*, vol. 10, pp. 19-48, 2003.
- [12] A. Belarbi and H. Wang, "Bond durability of FRP bars embedded in fiber-reinforced concrete," *Journal of composites for construction*, vol. 16, pp. 371-380, 2012.
- [13] B. Benmokrane, A. H. Ali, H. M. Mohamed, A. ElSafty, and A. Manalo, "Laboratory assessment and durability performance of vinyl-ester, polyester, and epoxy glass-FRP bars for concrete structures," *Composites Part B: Engineering*, vol. 114, pp. 163-174, 2017.
- [14] G. Nkurunziza, A. Debaiky, P. Cousin, and B. Benmokrane, "Durability of GFRP bars: A critical review of the literature," *Progress in structural engineering and materials*, vol. 7, pp. 194-209, 2005.

- [15] J. F. Davalos, Y. Chen, and I. Ray, "Effect of FRP bar degradation on interface bond with high strength concrete," *Cement and Concrete Composites*, vol. 30, pp. 722-730, 2008.
- [16] F. Ceroni, E. Cosenza, M. Gaetano, and M. Pecce, "Durability issues of FRP rebars in reinforced concrete members," *Cement and concrete composites*, vol. 28, pp. 857-868, 2006.
- [17] V. M. Karbhari and G. Xian, "Hygrothermal effects on high VF pultruded unidirectional carbon/epoxy composites: Moisture uptake," *Composites Part B: Engineering*, vol. 40, pp. 41-49, 2009.
- [18] H.-Y. Kim, Y.-H. Park, Y.-J. You, and C.-K. Moon, "Short-term durability test for GFRP rods under various environmental conditions," *Composite structures*, vol. 83, pp. 37-47, 2008.
- [19] H. Saadatmanesh, "Fiber composites for new and existing structures," *ACI Structural Journal*, vol. 91, pp. 346-354, 1994.
- [20] B. Benmokrane and B. Tighiouart, "Bond strength and load distribution of composite GFRP reinforcing bars in concrete," *Materials Journal*, vol. 93, pp. 254-259, 1996.
- [21] O. Chaallal and B. Benmokrane, "Pullout and bond of glass-fibre rods embedded in concrete and cement grout," *Materials and structures*, vol. 26, pp. 167-175, 1993.
- [22] B. Tighiouart, B. Benmokrane, and D. Gao, "Investigation of bond in concrete member with fibre reinforced polymer (FRP) bars," *Construction and building materials*, vol. 12, pp. 453-462, 1998.
- [23] W. Tang, T. Lo, and R. V. Balendran, "Bond performance of polystyrene aggregate concrete (PAC) reinforced with glass-fibre-reinforced polymer (GFRP) bars," *Building and Environment*, vol. 43, pp. 98-107, 2008.
- [24] M. Bazli, X.-L. Zhao, Y. Bai, R. S. Raman, and S. Al-Saadi, "Bond-slip behaviour between FRP tubes and seawater sea sand concrete," *Engineering Structures*, vol. 197, p. 109421, 2019.
- [25] A. N. Dancygier, A. Katz, and U. Wexler, "Bond between deformed reinforcement and normal and high-strength concrete with and without fibers," *Materials and Structures*, vol. 43, pp. 839-856, 2010.
- [26] J.-P. Won, C.-G. Park, H.-H. Kim, S.-W. Lee, and C.-I. Jang, "Effect of fibers on the bonds between FRP reinforcing bars and high-strength concrete," *Composites Part B: Engineering*, vol. 39, pp. 747-755, 2008.
- [27] J. Bilcik and I. Holly, "Effect of reinforcement corrosion on bond behaviour," *Procedia Engineering*, vol. 65, pp. 248-253, 2013.
- [28] M. Harajli and M. Abouniaj, "Bond performance of GFRP bars in tension: Experimental evaluation and assessment of ACI 440 guidelines," *Journal of Composites for Construction*, vol. 14, pp. 659-668, 2010.
- [29] N. Gažovičová, J. Bilčík, I. Hollý, and J. Halvonik, "Bond Behaviour between GFRP Reinforcement and Concrete Using a Pull-Out Test," in *Solid State Phenomena*, 2018, pp. 232-237.
- [30] D. Szczech and R. Kotynia, "Beam bond tests of GFRP and steel reinforcement to concrete," *Archives of Civil Engineering*, vol. 64, pp. 243-256, 2018.

- [31] H. V. GangaRao, N. Taly, and P. Vijay, *Reinforced concrete design with FRP composites*: CRC press, 2006.
- [32] R. Whittle, *Failures in concrete structures: case studies in reinforced and prestressed concrete*: Crc Press, 2012.
- [33] R. Masmoudi, A. Masmoudi, M. B. Ouezdou, and A. Daoud, "Long-term bond performance of GFRP bars in concrete under temperature ranging from 20 C to 80 C," *Construction and Building Materials*, vol. 25, pp. 486-493, 2011.
- [34] A. Richardson and P. Drew, "Fibre reinforced polymer and steel rebar comparative performance," *Structural Survey*, 2011.
- [35] L. J. Malvar, J. Cox, and K. B. Cochran, "Bond between carbon fiber reinforced polymer bars and concrete. I: Experimental study," *Journal of composites for construction*, vol. 7, pp. 154-163, 2003.
- [36] S. Islam, H. M. Afefy, K. Sennah, and H. Azimi, "Bond characteristics of straight-and headed-end, ribbed-surface, GFRP bars embedded in high-strength concrete," *Construction and Building Materials*, vol. 83, pp. 283-298, 2015.
- [37] Y. Ding, X. Ning, Y. Zhang, F. Pacheco-Torgal, and J. Aguiar, "Fibres for enhancing of the bond capacity between GFRP rebar and concrete," *Construction and Building Materials*, vol. 51, pp. 303-312, 2014.
- [38] X. Lin and Y. Zhang, "Bond–slip behaviour of FRP-reinforced concrete beams," *Construction and Building Materials*, vol. 44, pp. 110-117, 2013.
- [39] E. Cosenza, G. Manfredi, and R. Realfonzo, "Development length of FRP straight rebars," *Composites Part B: Engineering*, vol. 33, pp. 493-504, 2002.
- [40] R. Okelo and R. L. Yuan, "Bond strength of fiber reinforced polymer rebars in normal strength concrete," *Journal of composites for construction*, vol. 9, pp. 203-213, 2005.
- [41] J. Larralde and R. Silva-Rodriguez, "Bond and slip of FRP rebars in concrete," *Journal of Materials in Civil Engineering*, vol. 5, pp. 30-40, 1993.
- [42] E. M. Golafshani, A. Rahai, and M. H. Sebt, "Bond behavior of steel and GFRP bars in self-compacting concrete," *Construction and Building Materials*, vol. 61, pp. 230-240, 2014.
- [43] A. Nanni, C. Bakis, and T. Boothby, "Test methods for FRP-concrete systems subjected to mechanical loads: state of the art review," *Journal of Reinforced Plastics and Composites*, vol. 14, pp. 524-558, 1995.
- [44] F. Shahidi, L. Wegner, and B. Sparling, "Investigation of bond between fibre-reinforced polymer bars and concrete under sustained loads," *Canadian Journal of Civil Engineering*, vol. 33, pp. 1426-1437, 2006.
- [45] M. Esfandeh, A. R. Sabet, A. M. Rezadoust, and M. B. Alavi, "Bond performance of FRP rebars with various surface deformations in reinforced concrete," *Polymer composites*, vol. 30, pp. 576-582, 2009.
- [46] M. Antonietta Aiello, M. Leone, and M. Pecce, "Bond performances of FRP rebars-reinforced concrete," *Journal of materials in civil engineering*, vol. 19, pp. 205-213, 2007.
- [47] Z. Achillides and K. Pilakoutas, "Bond behavior of fiber reinforced polymer bars under direct pullout conditions," *Journal of Composites for construction*, vol. 8, pp. 173-181, 2004.

- [48] E. Cosenza, G. Manfredi, and R. Realfonzo, "Behavior and modeling of bond of FRP rebars to concrete," *Journal of composites for construction*, vol. 1, pp. 40-51, 1997.
- [49] M. Baena, L. Torres, A. Turon, and C. Barris, "Experimental study of bond behaviour between concrete and FRP bars using a pull-out test," *Composites Part B: Engineering*, vol. 40, pp. 784-797, 2009.
- [50] L. J. Malvar, "Bond stress-slip characteristics of FRP rebars," Naval Facilities Engineering Service Center Port Hueneme CA1994.
- [51] C. Wu, Y. Bai, and S. Kwon, "Improved bond behavior between GFRP rebar and concrete using calcium sulfoaluminate," *Construction and Building Materials*, vol. 113, pp. 897-904, 2016.
- [52] R. A. Goraya, K. Ahmed, and M. A. Tahir, "Effect of surface texture on bond strength of GFRP rebar in concrete," *Mehran University Research Journal of Engineering & Technology*, vol. 30, pp. 45-52, 2011.
- [53] G. Fava, V. Carvelli, and M. A. Pisani, "Remarks on bond of GFRP rebars and concrete," *Composites Part B: Engineering*, vol. 93, pp. 210-220, 2016.
- [54] F. Yan, Z. Lin, and M. Yang, "Bond mechanism and bond strength of GFRP bars to concrete: A review," *Composites Part B: Engineering*, vol. 98, pp. 56-69, 2016.
- [55] B. McCallum, "Experimental evaluation of the bond dependent coefficient and parameters which influence crack width in GFRP reinforced concrete," 2013.
- [56] R. Okelo, "Realistic bond strength of FRP rebars in NSC from beam specimens," *Journal of Aerospace Engineering*, vol. 20, pp. 133-140, 2007.
- [57] ACI, "Guide for the design and construction of structural concrete reinforced with FRP bars," in *ACI 440.1 R-06*, ed, 2006.
- [58] L. B. D. Specifications, "American Association of State Highway and Transportation Officials (AASHTO)," *Washington, DC, USA*, 2012.
- [59] A. G. Razaqpur, B. O. Isgor, S. Greenaway, and A. Selley, "Concrete contribution to the shear resistance of fiber reinforced polymer reinforced concrete members," *Journal of Composites for Construction*, vol. 8, pp. 452-460, 2004.
- [60] H. M. Mohamed and R. Masmoudi, "Axial load capacity of concrete-filled FRP tube columns: Experimental versus theoretical predictions," *Journal of composites for construction*, vol. 14, pp. 231-243, 2010.
- [61] T. Nagasaka, H. Fukuyama, and M. Tanigaki, "Shear performance of concrete beams reinforced with FRP stirrups," *Special publication*, vol. 138, pp. 789-812, 1993.
- [62] L. Taerwe, *Non-Metallic (FRP) Reinforcement for Concrete Structures: Proceedings of the Second International RILEM Symposium* vol. 29: CRC Press, 1995.
- [63] A. De Luca and A. Nanni, "FRP-reinforced concrete structures," *Wiley encyclopedia of composites*, pp. 1-14, 2011.
- [64] H. J. Dagher, T. E. Kimball, S. M. Shaler, and B. Abdel-Magid, "Effect of FRP reinforcement on low grade eastern hemlock glulams," in *Proceedings of the National Conference on Wood in Transportation Structures*, 1996, pp. 207-214.
- [65] S. Tottori and H. Wakui, "Shear capacity of RC and PC beams using FRP reinforcement," *Special Publication*, vol. 138, pp. 615-632, 1993.

- [66] J. R. Yost, S. P. Gross, and D. W. Dinehart, "Shear strength of normal strength concrete beams reinforced with deformed GFRP bars," *Journal of composites for construction*, vol. 5, pp. 268-275, 2001.
- [67] A. Committee, "Building code requirements for structural concrete (ACI 318-05) and commentary (ACI 318R-05)," 2005.
- [68] J. Valivonis, M. Budvytis, M. Atutis, E. Atutis, and L. Juknevičius, "Study on shear resistance of fiberreinforced polymer–reinforced concrete beams," *Advances in Mechanical Engineering*, vol. 7, p. 1687814015593873, 2015.
- [69] E. Shehata, R. Morphy, and S. Rizkalla, "Fibre reinforced polymer shear reinforcement for concrete members: behaviour and design guidelines," *Canadian Journal of Civil Engineering*, vol. 27, pp. 859-872, 2000.
- [70] A. Elbana, M. T. Junaid, and S. Altoubat, "Flexural behavior and strengthening of geopolymer concrete beams reinforced with GFRP bars using CFRP sheets," in *SynerCrete'18 International Conference on Interdisciplinary Approaches for Cement-based Materials and Structural Concrete*, 2018, pp. 449-454.
- [71] M. T. Junaid, A. Elbana, S. Altoubat, and Z. Al-Sadoon, "Experimental study on the effect of matrix on the flexural behavior of beams reinforced with Glass Fiber Reinforced Polymer (GFRP) bars," *COMPOSITE STRUCTURES*, vol. 222, 2019.
- [72] M. T. Junaid, A. Elbana, and S. Altoubat, "Flexural response of geopolymer and fiber reinforced geopolymer concrete beams reinforced with GFRP bars and strengthened using CFRP sheets," in *Structures*, 2020, pp. 666-677.
- [73] M. T. Junaid, A. Elbana, S. Altoubat, and Z. Al-Sadoon, "Experimental study on the effect of matrix on the flexural behavior of beams reinforced with Glass Fiber Reinforced Polymer (GFRP) bars," *Composite Structures*, vol. 222, p. 110930, 2019.
- [74] A. Nanni, "Flexural behavior and design of reinforced concrete using FRP rods," *Journal of Structural Engineering*, vol. 119, pp. 3344-3359, 1993.
- [75] S. S. Faza and H. V. Gangarao, "Theoretical and experimental correlation of behavior of concrete beams reinforced with fiber reinforced plastic rebars," *Special Publication*, vol. 138, pp. 599-614, 1993.
- [76] L. Jaejer, A. Mufti, and G. Tadros, "The concept of the overall performance factor in rectangular-section reinforced concrete beams," in *Proceedings of the 3rd international symposium on non-metallic (FRP) reinforcement for concrete structures*, 1997, pp. 551-558.
- [77] T. Alkhrdaji, E. R. Fyfe, J. Korff, M. Schupack, C. E. Bakis, T. R. Gentry, *et al.*, "Guide for the Design and Construction of Structural Concrete Reinforced with FRP Bars," 2006.
- [78] W. Zhao, K. Maruyama, and H. Suzuki, "Shear behavior of concrete beams reinforced by FRP rods as longitudinal and shear reinforcement," in *Rilem Proceedings*, 1995, pp. 352-352.
- [79] A. Machida and T. Uomoto, *Recommendation for design and construction of concrete structures using continuous fiber reinforcing materials*: Japan Soc. of Civil Engineers, 1997.
- [80] Y. Sonobe, H. Fukuyama, T. Okamoto, N. Kani, K. Kimura, K. Kobayashi, *et al.*, "Design guidelines of FRP reinforced concrete building structures," *Journal of composites for Construction*, vol. 1, pp. 90-115, 1997.

- [81] C. R. Michaluk, S. H. Rizkalla, G. Tadros, and B. Benmokrane, "Flexural behavior of one-way concrete slabs reinforced by fiber reinforced plastic reinforcements," *ACI structural Journal*, vol. 95, pp. 353-365, 1998.
- [82] A. K. Tureyen and R. J. Frosch, "Shear tests of FRP-reinforced concrete beams without stirrups," *Structural Journal*, vol. 99, pp. 427-434, 2002.
- [83] J. Premalatha, R. Shanthi Vengadeshwari, and P. Srihari, "Finite element modeling and analysis of RC beams with GFRP and steel bars," *International Journal of Civil Engineering and Technology (IJCIET)*, vol. 8, pp. 671-679, 2017.
- [84] W. Qu, X. Zhang, and H. Huang, "Flexural behavior of concrete beams reinforced with hybrid (GFRP and steel) bars," *Journal of Composites for construction*, vol. 13, pp. 350-359, 2009.
- [85] L. Dahmani, A. Khennane, and S. Kaci, "Crack identification in reinforced concrete beams using ANSYS software," *Strength of materials*, vol. 42, pp. 232-240, 2010.
- [86] A. S. Mosallam and S. Banerjee, "Shear enhancement of reinforced concrete beams strengthened with FRP composite laminates," *Composites Part B: Engineering*, vol. 38, pp. 781-793, 2007.
- [87] X. Z. Zhang, L. L. Liu, and K. D. Tang, "Nonlinear Analysis of Reinforced Concrete Beam by ANSYS," in *Applied Mechanics and Materials*, 2013, pp. 663-666.
- [88] G. Vasudevan, S. Kothandaraman, and S. Azhagarsamy, "Study on non-linear flexural behavior of reinforced concrete beams using ANSYS by discrete reinforcement modeling," *Strength of materials*, vol. 45, pp. 231-241, 2013.
- [89] M. T. Junaid, A. Elbana, and S. Altoubat, "Predicting Flexural Capacity of Concrete Beams Reinforced with GFRP Bars and Strengthened with CFRP Sheets," in *In the 4th World Congress on Civil, Structural, and Environmental Engineering (CSEE'19)*, 2019, p. 153.
- [90] A. Elbana and M. T. Junaid, "Determination of flexural capacity for GFRP-reinforced concrete beams retrofitted using external CFRP sheet," in *Structures*, 2020, pp. 1384-1395.
- [91] M. T. Junaid, A. S. Karzad, and A. Elbana, "Experimental study on the shear behavior of GFRP reinforced concrete beams strengthened using CFRP sheets," in *IOP Conference Series: Materials Science and Engineering*, 2020, p. 012018.
- [92] M. T. Junaid, A. Elbana, and S. Altoubat, "Predicting Flexural Capacity of Concrete Beams Reinforced with GFRP Bars and Strengthened with CFRP Sheets."

“

# Appendix

..

## 8. Appendix

### 8.1. Appendix A

Calculations

Procedure	Calculation in SI units				
<b>1- Dimensions of the RC beam section:</b>	h (mm)	d (mm)	b (mm)	a (mm)	l (mm)
	300	250	200	30	2100
Cover = 30 mm ,					
<b>2- Calculation of gross moment of inertia:</b>  $I_g = \frac{bh^3}{12}$	Where b=200 and h=300  $I_g = \frac{(200)(300)^3}{12} = 450000000 \text{ mm}^4$				
<b>3- Compute the proportion among the modulus of elasticity for FRP rebar to the concrete modulus of elasticity</b>  <b>Check the crack width:</b>  $n_f = \frac{E_f}{E_c} = \frac{E_f}{4750\sqrt{f'_c}}$	Where $E_f = 60000 \text{ MPa}$ and $f'_c = 40.96 \text{ MPa}$  $n_f = \frac{E_f}{E_c} = \frac{60000}{4750\sqrt{40.96}} = 1.97$				

..

<p><b>4- Calculate “K” factor in the following equation:</b></p> $K = \sqrt{2\rho_f n_f + (\rho_f n_f)^2} - \rho_f n_f$	<p>Where <math>\rho_f = 0.00726</math></p> $K = \sqrt{2(0.00726)(1.97) + (0.00726 * 1.97)^2} - (0.00726)(1.97) = 0.156$
<p><b>5- Calculate the moment of inertia of the transformed cracked section of the beam:</b></p> $I_{cr} = \frac{bd^3}{3} K^3 + n_f A_f d^2 (1 - K)^2$	<p>Where <math>A_f = 363 \text{ mm}^2</math></p> $I_{cr} = \frac{(200)(250)^3}{3} (0.156)^3 + (1.97)(363)(250)^2 (1 - 0.156)^2 = 35851451.7 \text{ mm}^4$
<p><b>6- Compute cracked section properties:</b></p> $f_r = 0.62\sqrt{f'_c}$	<p>Where <math>f'_c = 40.96 \text{ MPa}</math></p> $f_r = 0.62\sqrt{40.96} = 3.968 \text{ MPa}$

..

<p><b>7- Calculate the cracking moment:</b></p> $M_{cr} = \frac{2f_r I_g}{h}$	$M_{cr} = \frac{2(3.96)(450000000)}{300} = 11.904 \text{ kN.m}$
<p><b>8-compute the modification factor <math>\beta_d</math>:</b></p> $\beta_d = \frac{1}{5} \left[ \frac{\rho_f}{\rho_{fb}} \right]$	<p>Where <math>\rho_{fb} = 0.00625</math></p> $\beta_d = \frac{1}{5} \left[ \frac{0.00726}{0.00625} \right] = 0.2324$
<p><b>9- The equation can calculate the deflection due to applied load:</b></p> $(I_e) = \left( \frac{M_{cr}}{M_a} \right)^3 \beta_d I_g + \left[ 1 - \left( \frac{M_{cr}}{M_a} \right)^3 \right] I_{cr}$	<p>Where <math>M_a = 60.4</math></p> $(I_e) = \left( \frac{11.904}{60.4} \right)^3 (0.232)(450000000) + \left[ 1 - \left( \frac{11.904}{60.4} \right)^3 \right] 35851451.7 = 35577085.26 \text{ mm}^4$

..

<b>10-The delta calculates by :</b>	
$(\Delta_i) = \frac{5Ml^2}{48E_c(I_e)}$	$(\Delta_i) = \frac{5(60.4)(2100)^2}{48(4750\sqrt{40.96})(35577085.26)} = 25.9 \text{ mm}$

## 8.2. Appendix B

Step No 1: Fill in the blanks for the details in two columns in the Excel program. As shown in the Figure below.

	A	B
1		
2	Experimental mid span	
3	Deflection (mm)	Load (KN)
4	0	0.105
5	1	28.095
6	2	34.125
7	3	40.605
8	4	47.7
9	5	52.605
10	6	58.38
11	7	64.26

Step No 2: Choose any blank cell.

F	G

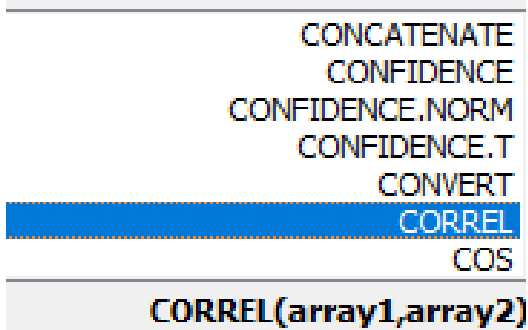
Step No 3: On the ribbon, click the feature button.

..



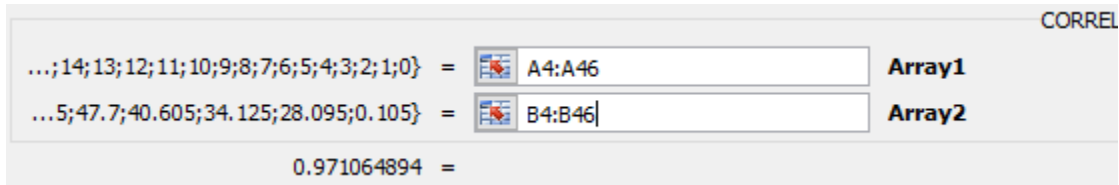
Step No 4: In the ‘Search for a feature’ box, type “correlation.”

Step No 5: Click the “Go” button. The word CORREL will be illuminated.



Step No 6: Press “OK.”

Step No 7: Fill in the “Array 1” and “Array 2” boxes with the position of your data.



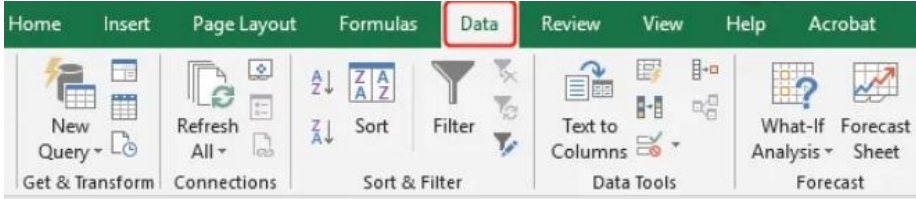
Step No 7: Press “OK.” The outcome will look in the cell which has been chosen in step No 2.



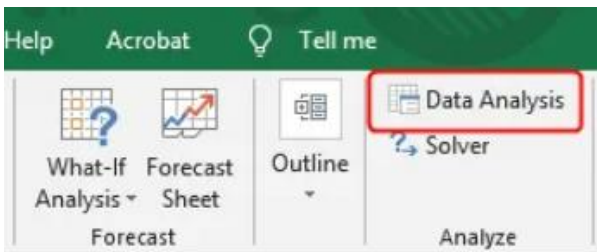
..

### 8.3.Appendix C

Step No1: Move to the Data Tab



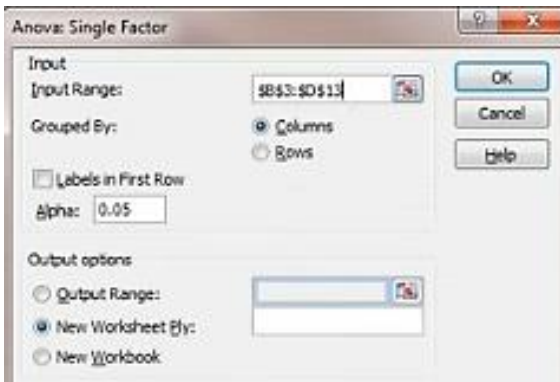
Step No2: Select Data Analysis from the menu.



Step No3: Click Ok after selecting Anova: Single-factor.

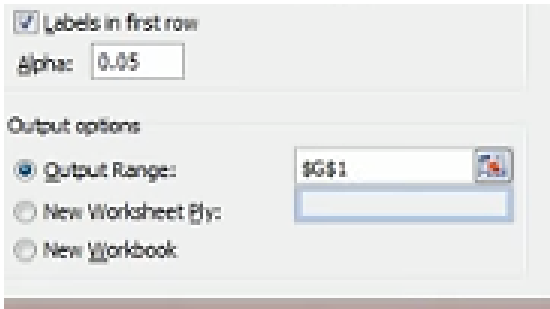


Step No4: Create a list by clicking the Input Range box.



Step No5: Find the output range by clicking the Output range box and then clicking Ok.

..



Step No6: The outcome will be shown in the excel sheet.

Anova: Single Factor						
SUMMARY						
Groups	Count	Sum	Average	Variance		
Load (KN) Expermeint	43	4990.47	116.0574419	2165.436985		
	0	0	#DIV/0!	#DIV/0!		
ANSYS	43	5108.8713	118.8109605	1747.750211		
ACI	31	3385.27	109.2022581	1810.791848		
ANOVA						
Source of Variation	SS	df	MS	F	F-value	Fcrit
Between Groups	1707.122819	3	569.0409398	0.294047589	0.829627402	2.684915784
Within Groups	218677.6177	113	1935.200156			
Total	220384.7405	116				